Comparisons of cell proliferation and cell death from tornaria larva to juvenile worm in the hemichordate *Schizocardium californicum*

Paul Bump[1], Margarita Khariton[2], Clover Stubbert[3], Nicole E. Moyen[1], Jia Yan[4], Bo Wang[2] and Christopher J. Lowe[1*]

Abstract

Background: There are a wide range of developmental strategies in animal phyla, but most insights into adult body plan formation come from direct-developing species. For indirect-developing species, there are distinct larval and adult body plans that are linked together by metamorphosis. Some outstanding questions in the development of indirect-developing organisms include the extent to which larval tissue undergoes cell death during the process of metamorphosis and when and where the tissue that will give rise to the adult originates. How do the processes of cell division and cell death redesign the body plans of indirect developers? In this study, we present patterns of cell proliferation and cell death during larval body plan development, metamorphosis, and adult body plan formation, in the hemichordate *Schizocardium californium* (Cameron and Perez in Zootaxa 3569:79–88, 2012) to answer these questions.

Results: We identified distinct patterns of cell proliferation between larval and adult body plan formation of *S. californicum*. We found that some adult tissues proliferate during the late larval phase prior to the start of overt metamorphosis. In addition, using an irradiation and transcriptomic approach, we describe a genetic signature of proliferative cells that is shared across the life history states, as well as markers that are unique to larval or juvenile states. Finally, we observed that cell death is minimal in larval stages but begins with the onset of metamorphosis.

Conclusions: Cell proliferation during the development of *S. californicum* has distinct patterns in the formation of larval and adult body plans. However, cell death is very limited in larvae and begins during the onset of metamorphosis and into early juvenile development in specific domains. The populations of cells that proliferated and gave rise to the larvae and juveniles have a genetic signature that suggested a heterogeneous pool of proliferative progenitors, rather than a set-aside population of pluripotent cells. Taken together, we propose that the gradual morphological transformation of *S. californicum* is mirrored at the cellular level and may be more representative of the development strategies that characterize metamorphosis in many metazoan animals.

Keywords: Metamorphosis, Hemichordate, Tornaria, Cell proliferation, Cell death

Background

The development of animal body plans has largely been informed by research in a few key model species that pattern the adult body plan during embryogenesis, a strategy termed direct development. However, this type of development is not representative of many animal groups, where embryogenesis gives rise to a larva with a

*Correspondence: clowe@stanford.edu
[1] Hopkins Marine Station, Department of Biology, Stanford University, Pacific Grove, CA, USA
Full list of author information is available at the end of the article

body plan distinct from that of the adult, a strategy called indirect development [2–4]. During direct development, the adult is formed directly from the embryo, while in indirect development, embryonic processes give rise to a larval body plan that later transforms into the adult. This transformation between larvae and adults is a developmental process known as metamorphosis, which is characterized by the loss of larval-specific structures and the emergence of adult structures [5–11]. The prevalence of this developmental strategy across animal phyla clearly demonstrates that a better mechanistic understanding of indirect development is critical for a more complete understanding of the developmental basis of body plan evolution.

Many marine organisms utilize indirect development, developing first as larvae that feed and grow before reaching metamorphosis [12, 13]. In species, such as gastropods with veliger larvae, the morphological difference between larval and adult body plans is not very pronounced, because in these organisms, metamorphosis represents a major shift in ecological niche but not a large morphological change [14, 15]. At the other end of the spectrum, as is found in some echinoids, larval and adult body plans can be radically different in organization with a "catastrophic metamorphosis." In this case, the adult develops as a rudiment within the larva and metamorphosis results in a complete reorganization of the body around new developmental axes in addition to the loss of larval structures [5, 16, 17]. Similarly, in some nemertean worms, with a pilidium larva, the adult develops from several rudiments, and metamorphosis culminates with the juvenile consuming the larval tissues [17, 18]. However, metamorphosis in species with distinct larval and adult body plans does not always involve a segregated rudiment or cataclysmic metamorphosis — instead larval tissue seems to be remodeled rapidly into the adult without obvious drastic histolysis of the larval body plan [2, 15, 19]. In this type of metamorphosis, do adult structures originate from a small population of proliferative cells? What is the fate of larval tissues? Indirect-developing hemichordates represent this particular type of metamorphosis and provide an opportunity to explore this type of developmental strategy.

Hemichordates are composed of two classes, the solitary enteropneust worms and the largely colonial, tube-dwelling pterobranchs [20–23]. While the position of hemichordates as sister to the echinoderms and closely related to chordates has been well established [24–27], new studies have challenged this position [28]. Within the enteropneusts, one family, the Harrimaniiidae, are direct developers, while the families Spengelidae and Ptychoderidae, are indirect developers with a distinct larval body plan called the tornaria. Morphological studies

of tornaria larvae and their counterpart adult bodies can be traced back to the late 1800s [29, 30] and more recent morphological descriptions of larval and adult body plans have been carried out in a range of enteropneust species; *Ptychodera flava* [31, 32], *Balanoglossus misakiensis* [33], *Balanoglossus simodensis* [34] and *S. californicum* [35]. In these species, the tornaria larva is formed following embryogenesis, while the benthic adult body plan forms by metamorphosis following an extended planktonic period [31, 33–36]. Studies of hemichordate complex life cycles have largely been based on morphological characters, with some descriptive patterning studies [37–53]. However, the cellular and developmental mechanisms through metamorphosis remain largely uncharacterized. For example, we do not know whether the adult is formed by transformation of larval tissues via transdifferentiation or by proliferation of adult-specific cells following large-scale larval cell death.
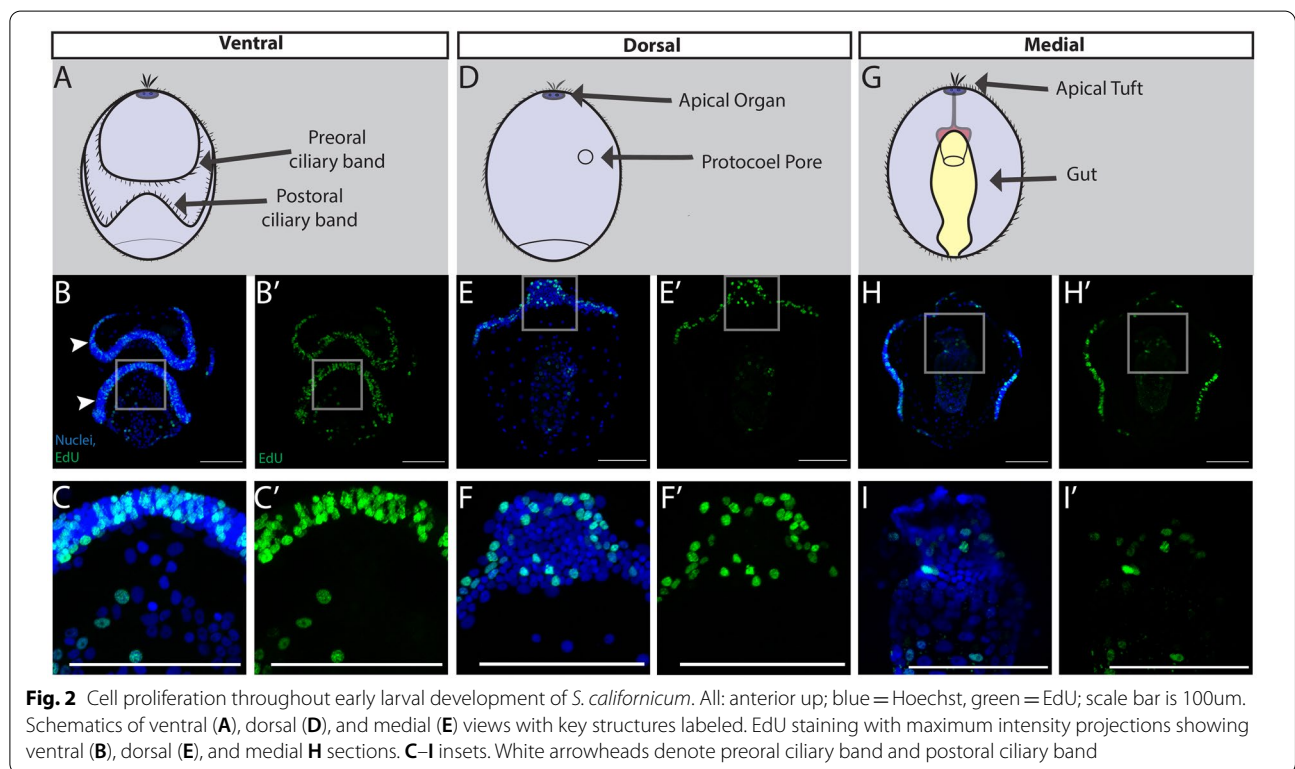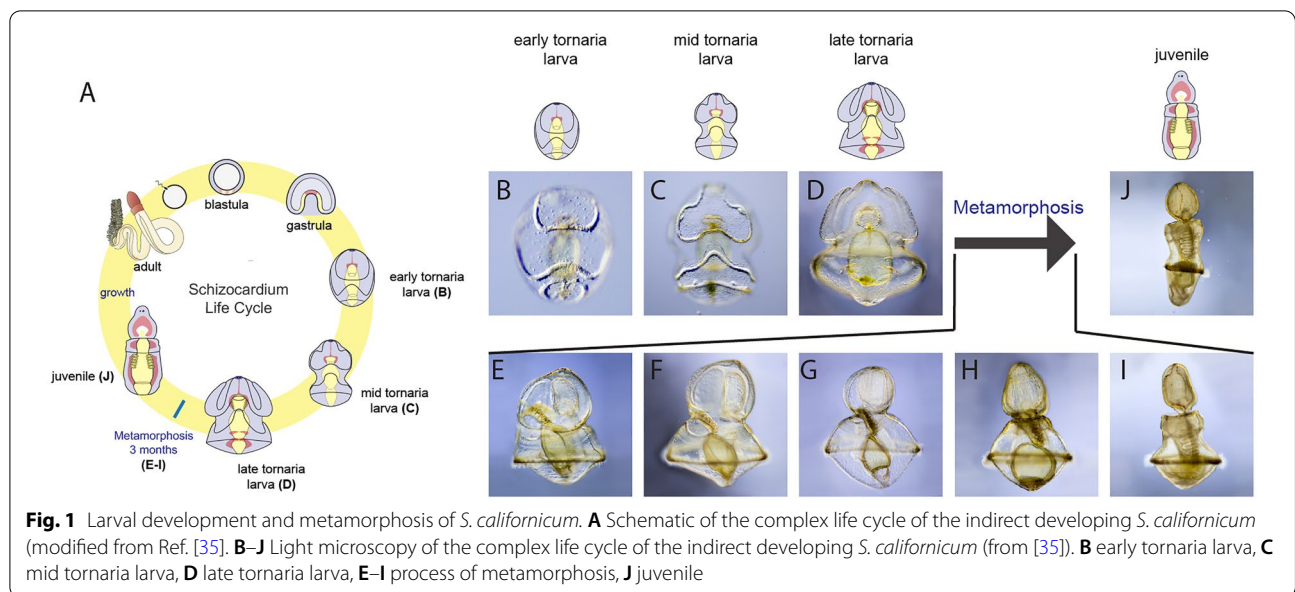
To begin to address these questions, we characterized proliferation and cell death through the development and metamorphosis of *S. californicum*. For the purpose of our study, we define metamorphosis in *S. californicum* as an overt morphological event. In a rapid 48-h period a swimming planktonic larva transforms into a burrowing benthic adult as larval ectoderm compacts and condenses over the underlying mesoderm and endoderm[35]. We found distinct patterns of cell proliferation between larval and adult body plans and that the start of a clear overt metamorphosis corresponded with an increase in cell death. To then determine if there were distinct genetic markers of proliferative cells, and if those markers differed between life history stages, we deployed an irradiation strategy to deplete proliferative cells and found a number of differentially expressed transcripts.

Results
Patterns of proliferation in larval and adult body plans.
We wanted to test whether patterns of cellular proliferation involved in the development of the planktonic larva were similar or different to those during the development of the benthic juvenile. To describe the distribution of proliferative cells throughout the development of *S. californicum,* we assessed the incorporation of the thymidine analog 5-ethynyl-29-deoxyuridine (EdU), which labels cells in S phase [54], during a range of developmental stages: early larval development (Fig. 1B), mid larval development (Fig. 1C), late larval development (Fig. 1D), metamorphosis (Fig. 1E–I), and in juvenile development (Fig. 1J).

The earliest larval developmental stage consists of a tightly packed ciliary band that loops around the larva, a thin wide squamous epithelium, an apical tuft, and a tripartite gut (Figs. 1B, 2). On the ventral surface we

Fig. 1 Larval development and metamorphosis of *S. californicum*. **A** Schematic of the complex life cycle of the indirect developing *S. californicum* (modified from Ref. [35]). **B**–**J** Light microscopy of the complex life cycle of the indirect developing *S. californicum* (from [35]). **B** early tornaria larva, **C** mid tornaria larva, **D** late tornaria larva, **E**–**I** process of metamorphosis, **J** juvenile

Fig. 2 Cell proliferation throughout early larval development of *S. californicum*. All: anterior up; blue = Hoechst, green = EdU; scale bar is 100um. Schematics of ventral (**A**), dorsal (**D**), and medial (**E**) views with key structures labeled. EdU staining with maximum intensity projections showing ventral (**B**), dorsal (**E**), and medial **H** sections. **C**–**I** insets. White arrowheads denote preoral ciliary band and postoral ciliary band

detected EdU$^+$ cells throughout the preoral and postoral loops of the circumoral ciliary band (Fig. 2B, C). The ciliary band is used for both swimming and particle capture at this stage [55–57] and makes up a large percentage of the ectoderm. We tested whether the ciliary bands were more prolif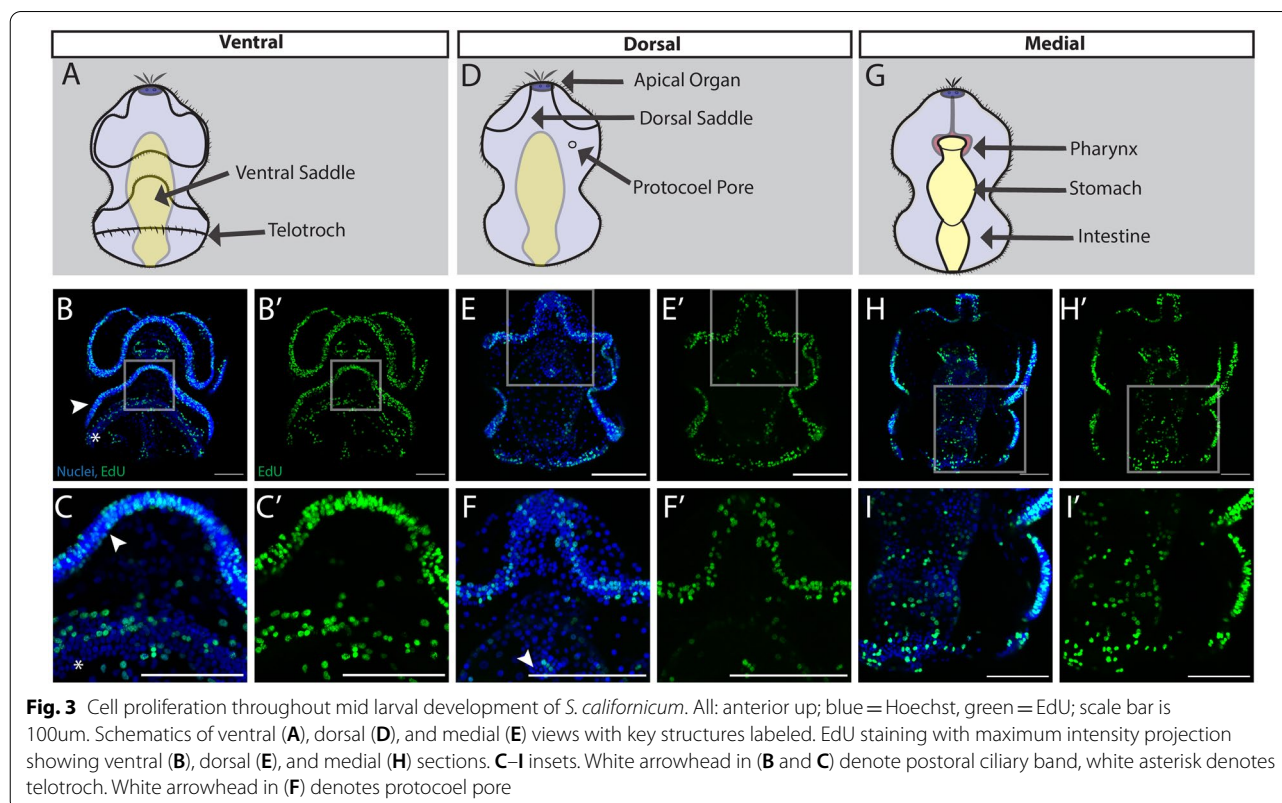erative than the general ectoderm, or simply had higher cell densities. The ciliary bands were densely packed with nuclei: there are ~59% greater number of cells in the ciliary bands versus all other tissues (paired t test, p = 0.016) and they were also more proliferative with ~22% more Edu$^+$ cells than all other tissues (paired t test, p = 0.008) (Additional file 1: S1A, B). This suggests

that while the ciliary bands are nuclei-dense regions, they appear to be some of those most proliferative structures at this stage. This pattern aligns with what has been observed in the ciliary bands of other Ambulacrarians, such as the bipinnaria larvae of *Pisaster ochraceus* and *Patiria miniata* [58]. On the dorsal side of the larva in the most anterior regions, EdU$^+$ cells were detected around the apical organ (Fig. 2E, F), a prominent structure of the larval nervous system [59–62]. Other important proliferative structures of larvae include the digestive tract, where microalgae that have been captured by the ciliary bands pass from the mouth into the pharynx, and finally into the stomach, where they are digested (Fig. 2H, I). In general, at this early larval stage most regions and tissues contain proliferative cells.

As the tornaria continues to grow and reaches the middle of larval development (Figs. 1C, 3), defined by the differentiation of dorsal and ventral saddles as well as the emergence of the posterior telotroch, proliferation continued throughout the ciliary bands. This was most apparent ventrally in the preoral and post-oral ciliary bands (Fig. 3B). Proliferative cells were detected in the developing telotroch, the posterior locomotory ciliary band (Fig. 3C). The telotroch is one of the most distinctive structures of the hemichordate tornaria with long compound cilia that beat to propel the larva through the water [57]. On the dorsal surface, the protocoel pore was

proliferative at this stage (Fig. 3E, F). This structure is a portion of the larval protonephridial system, an excretory system that uses a cilia-driven flow for ultrafiltration of coelomic fluid from the protocoel [63, 64]. Finally, at this stage the last notable structure is the tripartite gut, composed of pharynx, stomach and intestine, which continued to proliferate and grow (Fig. 3H, I).

Close to metamorphosis, the tornaria larva reach full size (~ 3 mm) and form two additional coelom pairs, the mesocoels and metacoels, and the precursors to the gill slits [65, 66] (Figs. 1D, 4), and we observed a notable shift in proliferative patterns from earlier developmental stages. Proliferative cells were still distributed throughout the ventral ectoderm, both in the ciliary bands, but now also more broadly in the squamous epithelium between the ciliary bands (Fig. 4B). There were also a number of EdU$^+$ cells distributed broadly throughout the posterior ectoderm of the larva, which is a territory that will compact and elongate during metamorphosis (Fig. 4C). Across the dorsal surface of the late larva, there were numerous proliferative cells distributed throughout the epithelium (Fig. 4E). There were EdU$^+$ cells throughout the telotroch and on either side of the dorsal midline, where the dorsal cord was beginning to form (Fig. 4F). Perhaps most interestingly, at this stage, the gut stopped proliferating and EdU$^+$ cells were detected within the forming

Fig. 3 Cell proliferation throughout mid larval development of *S. californicum*. All: anterior up; blue=Hoechst, green=EdU; scale bar is 100um. Schematics of ventral (**A**), dorsal (**D**), and medial (**E**) views with key structures labeled. EdU staining with maximum intensity projection showing ventral (**B**), dorsal (**E**), and medial (**H**) sections. **C**–**I** insets. White arrowhead in (**B** and **C**) denote postoral ciliary band, white asterisk denotes telotroch. White arrowhead in (**F**) denotes protocoel pore
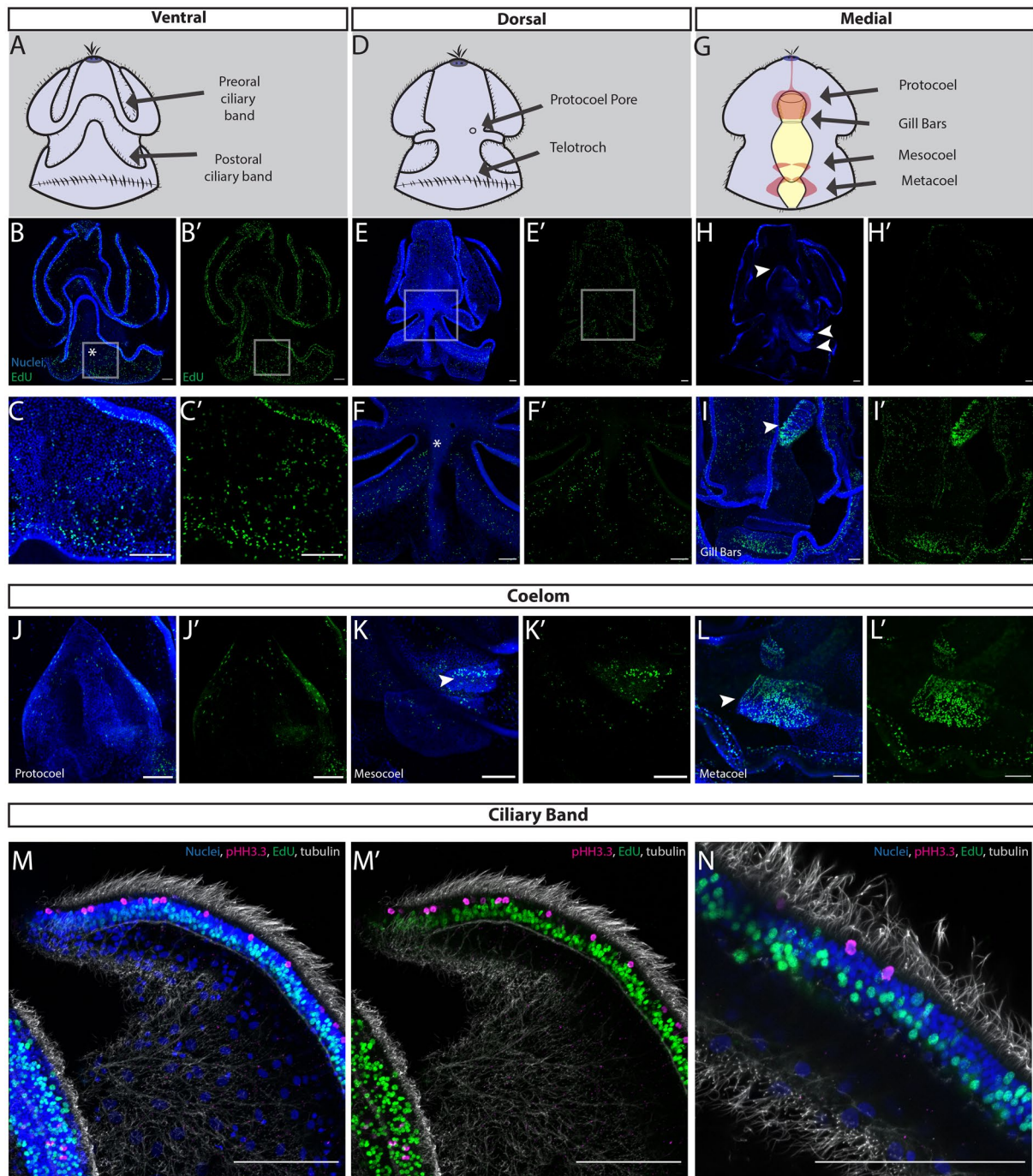
Fig. 4 Cell proliferation in late larval development of *S. californicum*. All: anterior up; blue = Hoechst, green = EdU; scale bar is 100 um. Schematics of ventral (**A**), dorsal (**D**), and medial (**G**) views with key structures labeled. EdU staining with maximum intensity projection ventral (**B**), dorsal (**E**), and medial (**H**) sections. **B** late larva ventral surface, **C** inset of (**B**), highlights ventral posterior epidermis and ciliary band **E** late larva dorsal surface, **F** inset of (**E**) highlights dorsal cord, marked by white asterisk, **H** late larva medial section, arrowheads highlight regions that will give rise to protocoel, mesocoel, and metacoel. **I** inset of lateral view of late larva medial section, arrowhead highlights gill bars. **J** protocoel, mesoderm that will form the proboscis, **K** mesocoel, mesoderm that will form the collar, **L** metacoel, mesoderm that will form the trunk. **M**, **N** distribution of anti-histone H3 (phospho S10) and EdU positive cells in ciliary bands, magenta = pHH3.3, grey = acetylated tubulin
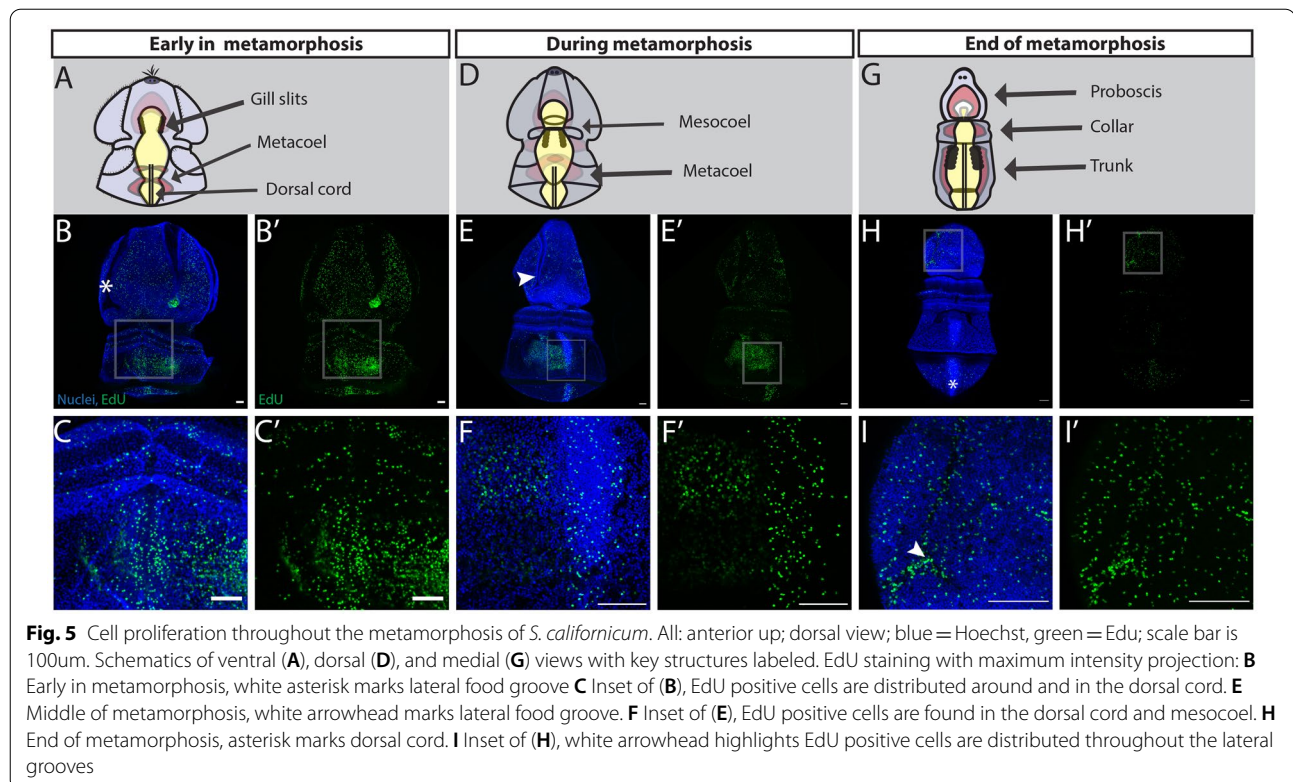
adult structures (Fig. 4H). In particular, we observed EdU$^+$ cells in the anlage of the gill slits, which are a prominent endomesoderm feature of the juvenile body plan that are not yet functional in the late larva [67] (Fig. 4I). EdU$^+$ cells were also enriched in the single anterior protocoel (Fig. 4J), and more posterior paired mesocoels (Fig. 4K) and metacoels (Fig. 4L), which will later form the adult mesodermal derivatives of the proboscis, collar, and trunk, respectively. In line with previous morphological observations, in late larvae, structures of the juvenile body plan began to proliferate to build the adult anatomical structures ahead of metamorphosis [35].

We also looked in more detail at the proliferative patterns in the ciliary band (Fig. 4M, N). To achieve this, we coupled our EdU detection with immunofluorescence staining of acetylated tubulin to visualize cilia and phosphorylated serine 10 of histone H3 (pHH3.3), which marks cells in G2/M phase. We found that proliferative cells display distinct spatial distribution with a row of EdU$^+$ cells at the base, then a row of differentiating phosophohistone h3.3 cells that are lateral to the cilia (Fig. 4M, N). This regional localization of EdU$^+$ cells in relationship to the differentiating phosophohistone h3.3 cells suggested that there could be a specific population of proliferative cells that give rise to the ciliary bands.

Proliferative patterns shift at metamorphosis

The first morphological indication of the onset of metamorphosis in *S. californicum* is the compaction and reorganization of the larval epidermis and an expansion of all the coeloms, which results in a decrease of the blastocoelar space (Fig. 1E, F) [35]. Early in metamorphosis, the ectoderm of the primary ventral lobe and primary dorsal lobe compact around the lateral food groove, as has been observed in *P. flava* [66], and EdU$^+$ cells were distributed throughout several regions of the ectoderm (Fig. 5B). EdU$^+$ cells were detected in the postoral field and primary dorsal saddle that give rise to both the proboscis and around the thickening collar (Fig. 5B). At this stage, EdU$^+$ cells were also found in the collar and posterodorsally in the region of the developing dorsal cord (Fig. 5C). On the ventral surface, EdU$^+$ cells showed a similar distribution to the dorsal side with proliferative cells in the preoral field, around the collar, in the anlage of the gill slits and in the epidermis, where the ventral cord eventually forms (Additional file 1: S1C).

Metamorphosis then proceeded with the prospective proboscis ectoderm continuing to thicken as the blastocoel was reduced, bringing it in contact with the expanding anterior coelom (Fig. 1G, H). The posterior ectoderm continued to expand as the forming trunk continued to elongate. At this stage, ectodermal proliferation continued in the general epidermis of the proboscis but was

Fig. 5 Cell proliferation throughout the metamorphosis of *S. californicum*. All: anterior up; dorsal view; blue = Hoechst, green = Edu; scale bar is 100um. Schematics of ventral (**A**), dorsal (**D**), and medial (**G**) views with key structures labeled. EdU staining with maximum intensity projection: **B** Early in metamorphosis, white asterisk marks lateral food groove **C** Inset of (**B**), EdU positive cells are distributed around and in the dorsal cord. **E** Middle of metamorphosis, white arrowhead marks lateral food groove. **F** Inset of (**E**), EdU positive cells are found in the dorsal cord and mesocoel. **H** End of metamorphosis, asterisk marks dorsal cord. **I** Inset of (**H**), white arrowhead highlights EdU positive cells are distributed throughout the lateral grooves

absent from the remnants of the ciliary bands (Fig. 5E). The epidermis of the proboscis transformed into a columnar organization as the larva began to take on a more vermiform shape. Other proliferative regions at this stage included the developing gill slits, the metacoels, and the dorsal cord (Fig. 5F). At this stage, proliferation on the ventral surface occurred in the anterior ectoderm, similar to the dorsal surface, absent from where the ciliary bands had been (Additional file 1: S1D). EdU$^+$ cells were also detected around the collar and around the field, where the ventral cord forms (Additional file 1: S1D).

Finally, metamorphosis concluded as the blastocoelar space of the proboscis was eliminated bringing the mesoderm and ectoderm in direct contact, the ectoderm of the proboscis and collar transformed into a columnar epithelium, and the posterior coeloms expanded and differentiated as the trunk was elongating and narrowing (Fig. 1I). At this stage, we detected proliferative cells specifically in the proboscis, the collar, dorsal cord, and more broadly below the telotroch in the most posterior ectoderm and mesoderm (Fig. 5H). In the proboscis ectoderm there were EdU$^+$ cells distributed throughout as well as a clear enrichment of EdU$^+$ cells in the lateral groove, the region that had previously been the larval food groove (Fig. 5I). A lateral view of this stage at metamorphosis, highlighted cell proliferation in the gill slits and gut as well as the dorsal and ventral midlines that give rise to the nerve cords (Additional file 1: S1E).

In three main regions of the newly formed juvenile (Fig. 1J), cell proliferation was detected in the proboscis, collar, gill pores, gill bars, and trunk (Fig. 6B). In the anterior of the juvenile, EdU$^+$ cells were localized to the epidermis and line the lateral groove and anterior collar (Fig. 6C). This region of the animal is highly innervated [35]. Proliferative cells were also found in the dorsal gill pores which have perforated to allow water flow through the gill slits and out the gill pores (Fig. 6D). Finally in the posterior of the newly formed juvenile, proliferative cells were located along the dorsal cord of the trunk (Fig. 6E). At this stage on the ventral surface, we detected EdU$^+$ cells in the proboscis, the gill slits, and in the ventral cord (Additional file 1: S1F). To see if these patterns of juvenile growth continued well after metamorphosis, we grew animals in sand for several weeks and repeated the EdU labeling, clearing the tissue to make it possible to visualize the distribution of proliferation in larger, thicker tissue. In continued juvenile growth (Fig. 6F) proliferative cells were found at the base of the collar coincident with serotonergic neurons [35]. Interestingly, at this later stage cell proliferation in the gill slits and dorsal cord was less pronounced, but a large number of EdU$^+$ cells were found mid-intestinal in the trunk, potentially identifying a new region of posterior growth [68].
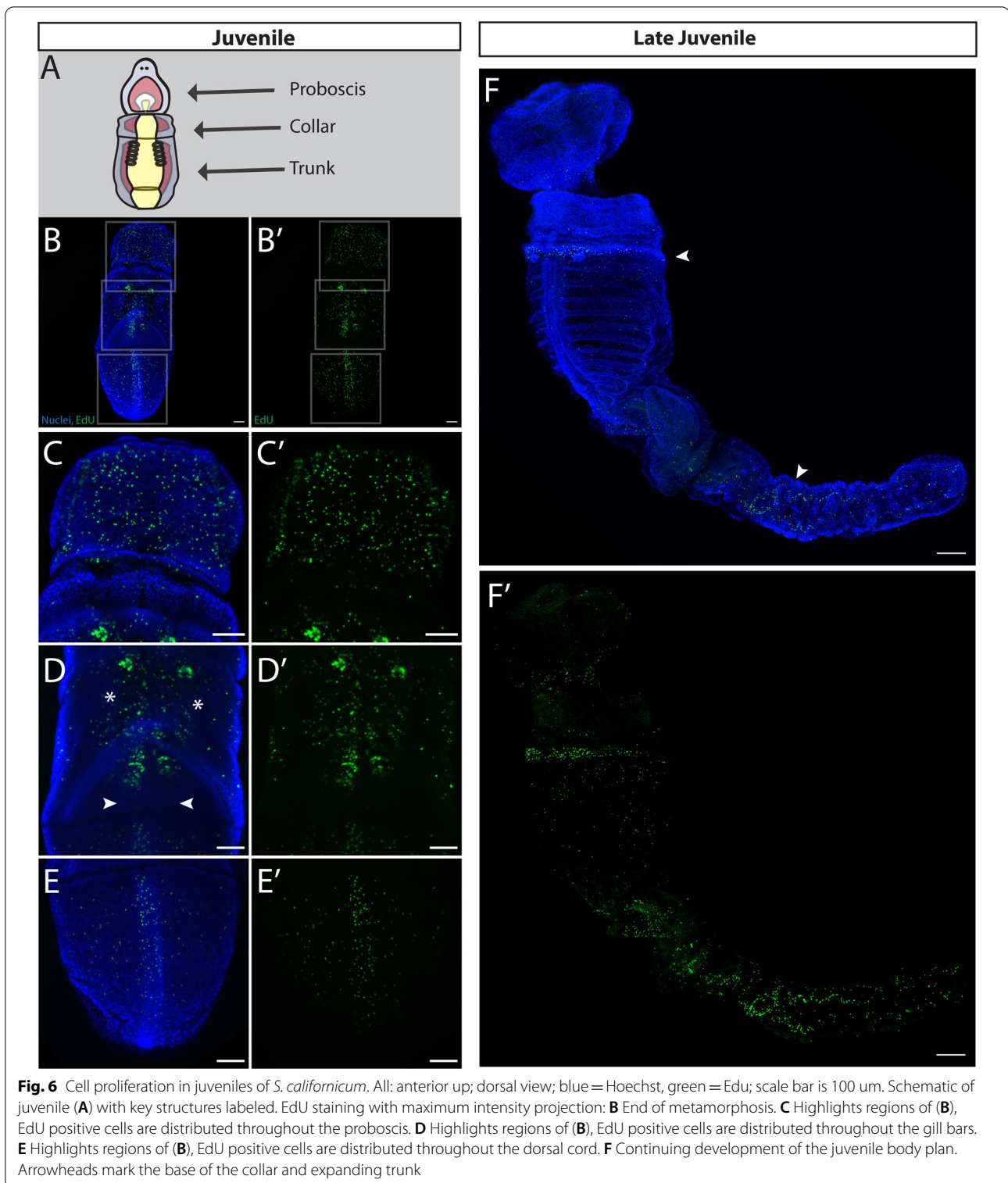
As *S. californicum* transitioned from a distinct larva through metamorphosis and into a juvenile, proliferative cells shifted in their distribution, restricting to specific regions in the juvenile body. Overall, our data suggests that the proliferation of the adult body plan begins at late larval stages prior to the start of the metamorphosis itself.

RNAseq after irradiation reveals the genetic signature of proliferative cells in two distinct life history states

To further explore the molecular characteristics of proliferative cells in *S. californicum*, we exploited the sensitivity of proliferative cells to irradiation [69–73]. We hypothesized that the transcripts of irradiation-sensitive genes would be restricted to our EdU$^+$, proliferative cell population. When we inspected the morphology of EdU$^+$ proliferative cells with fluorescent in situ hybridization (FISH) to detect histone h2b messenger RNA, a known cell cycle gene, we found that EdU$^+$ cells possess a narrow rim of cytoplasm of h2b mRNA surrounding their nucleus and these cells often display a cytoplasmic projection (Additional file 1: S1G, H). This morphology is reminiscent of the proliferative cells studied in other organisms, such as planarian neoblasts, which have been characterized as rounded mesenchymal cells with a high nuclear-to-cytoplasmic ratio that often extend a cytoplasmic projection [74, 75]. With these additional characterizations we next wanted to know if these proliferative cells might share any core genetic signatures with proliferative cells in other organisms. One hypothesis was that *S. californicum* would have a stem-cell-like population that expresses many of the classic multipotency or germline multipotency factors, such as *piwi, vasa,* and *nanos* [71, 76].

To do this, we treated larvae and juveniles with irradiation. Three days after treatment, animals looked morphologically the same as controls, but EdU incorporation was eliminated in both larvae and juveniles (Fig. 7A–D). We extracted total RNA from this same stage of three days post-irradiation from 5 pooled individuals in three independent biological replicates and made RNA sequencing libraries (Nugen-Tecan Genomics). RNAseq analysis of irradiated versus non-irradiated identified 20 genes in larvae and 123 genes in juveniles showing significant differential expression (log2 fold change ≥ -2) and p-adjusted value $\leq 10–6$ juveniles (Fig. 7E), with 5 genes that were downregulated at both stages.

In the larval stage, twenty candidate genes were specific, including *fgfr-B* (fibroblast growth factor receptor B) and a number of genes involved in cell division, such as *ince (*inner centromere protein) [77] *aspm-1* (abnormal spindle microtubule assembly*)* [78–80], and *dlgp5* (disks large-associated protein 5*)* [81, 82] (Additional

Fig. 6 Cell proliferation in juveniles of *S. californicum*. All: anterior up; dorsal view; blue = Hoechst, green = Edu; scale bar is 100 um. Schematic of juvenile (**A**) with key structures labeled. EdU staining with maximum intensity projection: **B** End of metamorphosis. **C** Highlights regions of (**B**), EdU positive cells are distributed throughout the proboscis. **D** Highlights regions of (**B**), EdU positive cells are distributed throughout the gill bars. **E** Highlights regions of (**B**), EdU positive cells are distributed throughout the dorsal cord. **F** Continuing development of the juvenile body plan. Arrowheads mark the base of the collar and expanding trunk

file 2: S2A). In juveniles, 123 genes showed significant differential expression including a potential germline marker *spne-2 (*spindle-E), genes involved in proliferation, such as *anln* (anilin), and genes related to a potential immune response *traf2* (TNF receptor-associated factor 2), *tlr2* (Toll-like receptor 2), and *tlr6* (Toll-like receptor 6) (Additional file 2: S2B).

Finally, five genes with differential expression were shared between larva and juvenile: *lbr-1* (Lamin B Receptor), *nusap* (Nucleolar And Spindle Associated Protein 1), *tenr-5* (Tenascin-R), *tlr6-1* (Toll-like receptor 6), and *unchar_4293* (an uncharacterized gene). *nusap* plays a role in spindle microtubule organization and also has been implicated in WNT signaling and metastasis [83], and *tenr-5* (Tenascin-R), which belongs to a group of extracellular matrix proteins, tenascins, which are important in vertebrates stem cell niches for tissue formation, cell adhesion modulation, and the regulation of proliferation and differentiation [84].

Among the larval irradiation-sensitive transcripts, *fgfr-B* was most notable. FGF receptors in vertebrates are known to regulate cell proliferation, differentiation, and play a key role in pluripotent stem cells [85]. The two hemichordate FGF receptors Fgfr-A and Fgfr-B arose from a hemichordate-specific duplication [86] and in the direct developing hemichordate *Saccoglossus kowalevskii, fgfr-B* is expressed in the endomesoderm at early gastrula stage and also in the ectoderm beginning at late gastrula into later stages [87]. In *S. californicum*, we examined the distribution of *fgfr-B* mRNA and found expression throughout regions, where we also had previously observed EdU$^+$ cells, particularly in the ciliary bands (Fig. 7G, H).

In the juvenile transcriptomes, the differential expression of *spne-2 (*spindle-E) was most notable. In *Drosophila melanogaster* spindle-E is involved in the generation of germ cell piwi-interacting-RNAs (piRNAs) and the DExD-box helicase domain of s*pindle-E* is required for silencing of transposable elements in the germline [88, 89]*.* In *S. californicum, spindle-E* was specifically expressed in mesenchymal cells around the posterior of the gills bars (Fig. 7I, K), which is consistent with Vasa expression in *P. flava* [90]. Given that *spindle-E* was expressed in a similar region and has been implicated in germline regulation, we hypothesize that *spindle-E* could potentially be a marker of proliferative germline cells in hemichordates.

The lamin B receptor gene, *lbr-1*, which plays an important role in tethering chromatin, was differentially expressed in the larval and juvenile stages. This suggests it may be a universal marker of proliferative cells in *S. californicum*. There are two types of chromatin attachment to lamina, one type is executed by the lamin B receptor in embryonic and non-differentiated cells, and the other by specific lamin a/c binding proteins in differentiated cells [91]. Previous work in ascidians and echinoderms has identified *lbr-1* orthologs and suggested that this gene may be unique to deuterostomes [92]. We examined the expression of *lbr-1* in larvae and found it localized in the ciliary bands (Fig. 7L, M), which we previously demonstrated were regions of active cellular proliferation (Fig. 3A). Similarly, at the juvenile stage we found *lbr-1* expression in a similar territory, where we had observed the distribution of EdU$^+$ cells (Figs. 5F, 6B, C), such as the lateral grooves in the proboscis (Fig. 7N, O) and in the gill bars (Fig. 7P). Our findings suggest that expression of *lbr-1* might serve as a useful marker of labeling proliferative cells across both life history states.
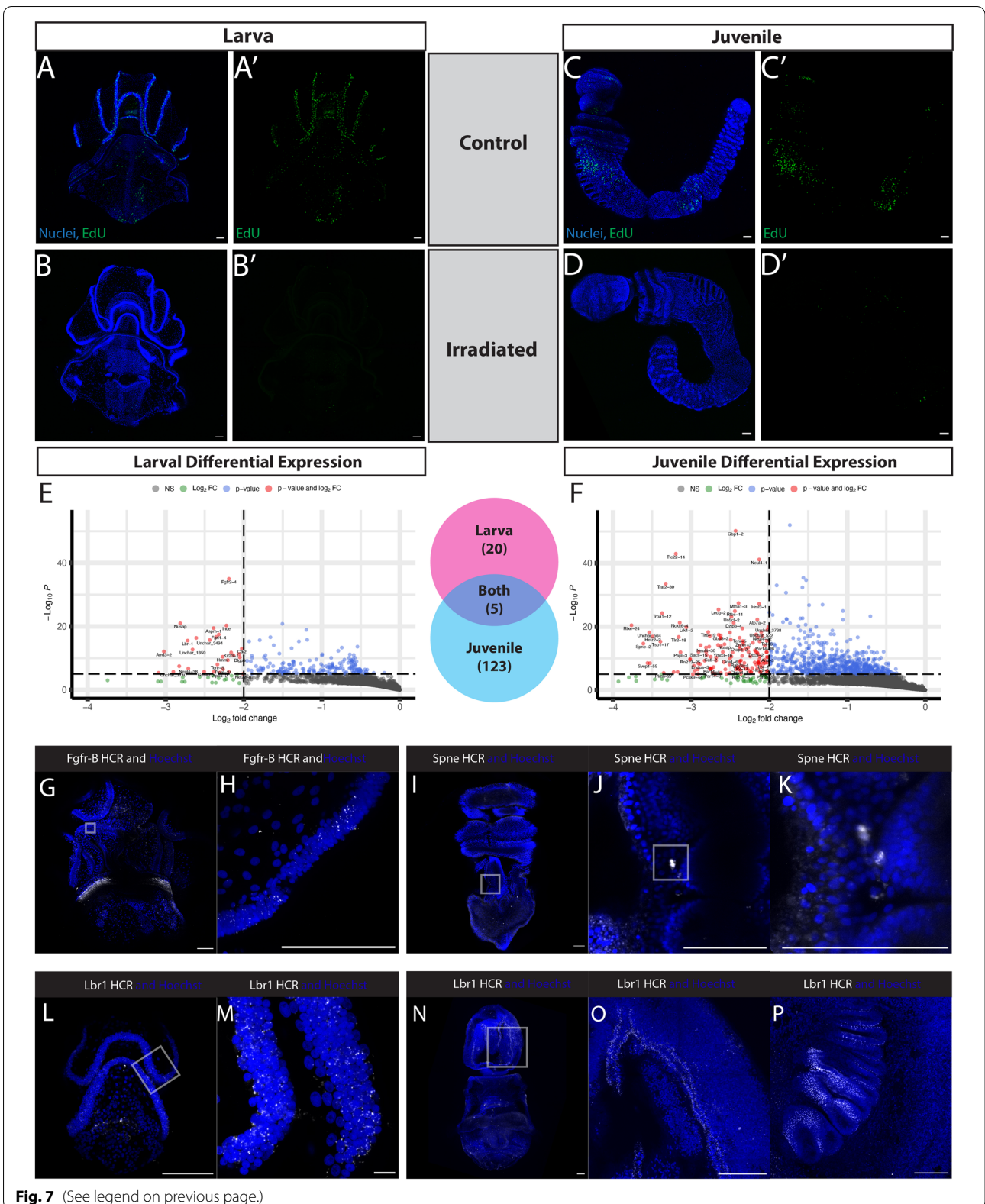
Finally, the classic multipotency or germline multipotency factors, such as *piwi, vasa,* and *nanos,* [71, 76] did not have significant differential expression (Additional file 2: S2C, D). Instead, what we recovered were genes related more to specific proliferative populations (*fgfr-B, spne-2,* and *lbr-1)* and thereby, revealed a possible heterogeneity among proliferative progenitor cells.

Cell death remodels larval tissue at metamorphosis

After an investigation of cell proliferation throughout the life cycle and metamorphosis of *S. californicum,* we next tested if patterns of proliferation were correlated with patterns of cell death. One larval structure that is lost or extensively remodeled at metamorphosis is the circumoral ciliary band, also called the longitudinal ciliary band, a larval specific feeding structure [57, 61] that is not retained in the juvenile. We investigated the distribution of cell death with TUNEL (terminal deoxynucleotidyl transferase dUTP nick end labeling), which detects breaks in DNA as a proxy for cells undergoing apoptosis [93]. The TUNEL assay labels all free 3′-hydoxyl termini meaning that TUNEL staining will detect apoptosis, programmed cell death, but also necrosis [94, 95]. We overcame previously limitations of TUNEL detection by taking advantage of Click-iT technology, which utilizes a
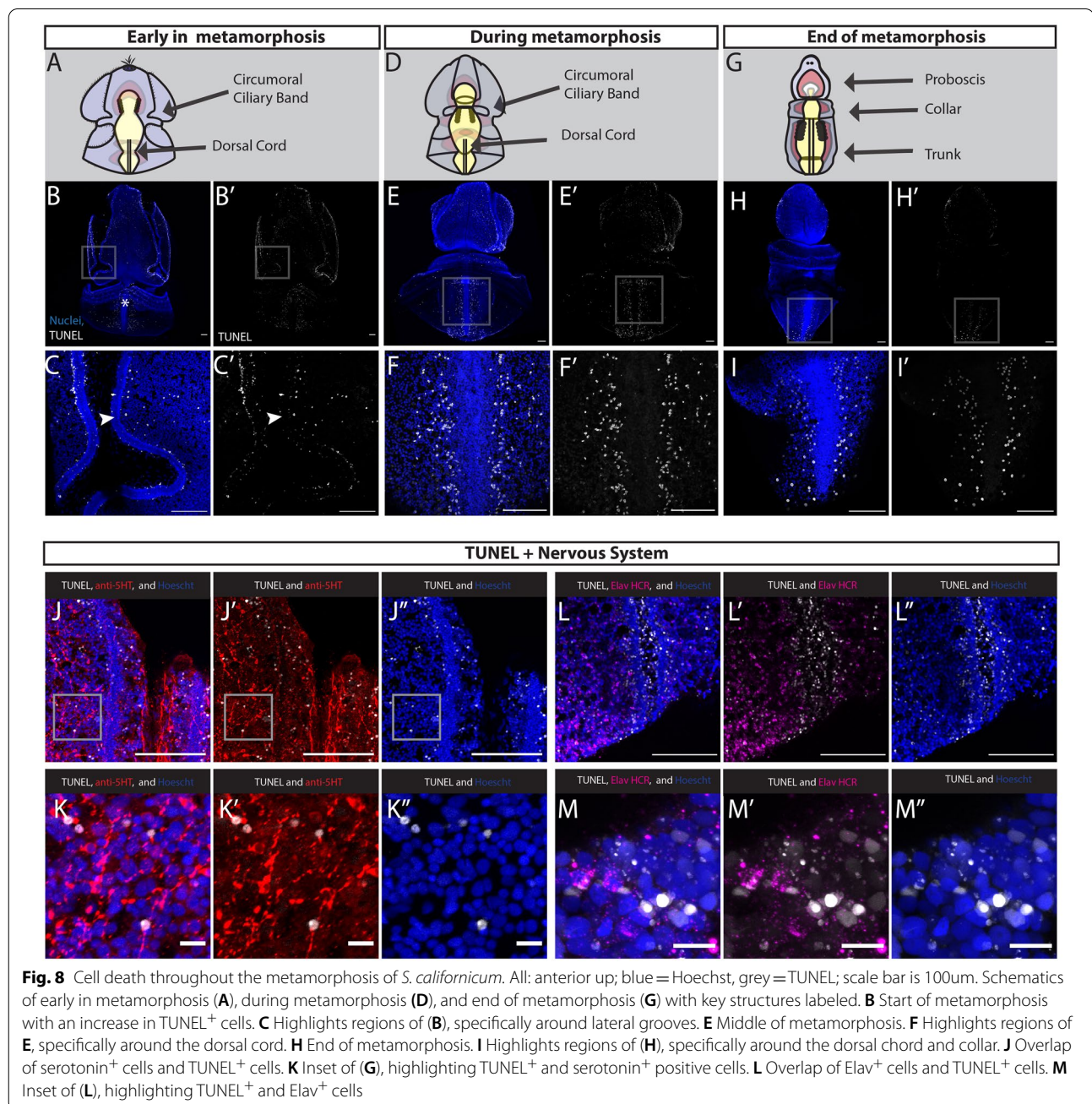

(See figure on next page.)

Fig. 7 Genetic signature of irradiation sensitive EdU cells in both larvae and juveniles. All; blue = Hoechst, green = EdU; scale bar is 100um. **A** Control larva representing the normal EdU pattern at this stage, representative of 5/5 animals. **B** Experimental larva representing the EdU pattern at this stage after receiving 120 Gy of X-ray irradiation, representative of 5/5 animals. **C** Control juvenile representing the normal EdU pattern at this stage, representative of 4/4 animals. **D** Experimental juvenile representing the EdU pattern at this stage after receiving 200 Gy of X-ray irradiation, representative of 2/2 animals. **E** Volcano plot showing expression differences in control versus irradiated larva. n = 3 for each group. **F** Volcano plot showing expression differences in control versus irradiated juvenile. n = 3 for each group. **G** A larva with HCR probes for Fgfr-B. **H** Higher magnification of ciliary band with Fgfr-B transcripts. **I** A juvenile with HCR probes for Spindle-E. **J**, **K** Higher magnification of Spindle-E transcripts expressed between the ectoderm and the gills bars. **L** A larva with HCR probes for Lbr-1. **M** Inset of H with Lbr-1 transcripts distributed throughout the ciliary band. **N** A juvenile with HCR probes for Lbr-1. **O** Inset of I with Lbr-1 transcripts distributed throughout the lateral grooves. **P** Lbr-1 transcripts distributed in the gill bars

Fig. 7 (See legend on previous page.)

modified dUTP with a small, bio-orthogonal alkyne moiety (EdUTP) and a copper catalyzed covalent click reaction between that alkyne and a picolyl azide dye [96, 97].

Throughout larval development and in late larva we detected few TUNEL$^+$ cells, suggesting very limited cell death at larval stages (Additional file 3: S3A–C). However, once metamorphosis began, indicated by the thickening of the larval epithelium, there was a large increase in TUNEL$^+$ cells (Fig. 8B). TUNEL$^+$ cells were distributed broadly throughout the ectoderm, with most of them on either side of the developing dorsal cord, and

in and around the circumoral ciliary band (Fig. 8C). The circumoral ciliary band was labelled with many TUNEL$^+$ cells, supporting the morphological observation that this structure begins to break down at this stage. There were a small number of TUNEL$^+$ at the anterior end of the protocoel (Additional file 3: S3D, E). TUNEL$^+$ cells were also absent from the gut at this stage, which is consistent with the morphological observation that the gut is maintained throughout the transition from larvae to adult [35]. To confirm adequate penetration of the TUNEL labeling into the deeper tissue layers, we performed a

Fig. 8 Cell death throughout the metamorphosis of *S. californicum*. All: anterior up; blue = Hoechst, grey = TUNEL; scale bar is 100um. Schematics of early in metamorphosis (**A**), during metamorphosis (**D**), and end of metamorphosis (**G**) with key structures labeled. **B** Start of metamorphosis with an increase in TUNEL$^+$ cells. **C** Highlights regions of (**B**), specifically around lateral grooves. **E** Middle of metamorphosis. **F** Highlights regions of **E**, specifically around the dorsal cord. **H** End of metamorphosis. **I** Highlights regions of (**H**), specifically around the dorsal chord and collar. **J** Overlap of serotonin$^+$ cells and TUNEL$^+$ cells. **K** Inset of (**G**), highlighting TUNEL$^+$ and serotonin$^+$ positive cells. **L** Overlap of Elav$^+$ cells and TUNEL$^+$ cells. **M** Inset of (**L**), highlighting TUNEL$^+$ and Elav$^+$ cells

positive control by artificially nicking the ends of DNA with DNAse-1 (Additional file 3: S3G, H).

At the mid-metamorphosis stage, TUNEL$^+$ cells were distributed throughout the epidermis and continue to label the disintegrating ciliary bands that fuse with each other (Fig. 8E). At this stage we continued to detect very few TUNEL$^+$ cells in the mesoderm and endoderm. The other region of the ectoderm, where the greatest number of TUNEL$^+$ cells were found is directly lateral to the dorsal nerve cord (Fig. 8F), a region where we observed many proliferative cells at the same stage. These general patterns that we see on the dorsal side are broadly similar to what was observed on the ventral surface with TUNEL$^+$ cells distributed in the ciliary bands and broadly in the ectoderm but excluded from the ventral nerve cord (Additional file 3: S3F). The presence of TUNEL$^+$ cells in and around the ciliary bands was consistent with a previous observation that the circumoral ciliary band degenerates and the serotonergic nervous system in this region undergoes extensive reorganization during metamorphosis, as neurite bundles that are present in the ciliary grooves disappear as the ciliary bands fuse [35, 98, 99].

At the end of metamorphosis, there were fewer TUNEL$^+$ cells detected. In the anterior, there were very few TUNEL$^+$ cells in either the ectoderm or mesoderm (Fig. 8H). Those TUNEL$^+$ cells that remain were scattered throughout the epidermis in the proboscis, but no longer in the lateral grooves, which from our EdU study we have observed becoming proliferative at this stage (Fig. 5F). In the posterior, the remaining TUNEL$^+$ cells were detected on either side of the dorsal cord, most prominently in the posterior, where the larval epidermis had compacted (Fig. 8I).

To understand the interaction of cell death with the nervous system, we examined serotonin localization along with TUNEL early in metamorphosis and found there is colocalization of serotonergic$^+$ cells with TUNEL$^+$ cells (Fig. 8J, K). We also examined expression of *elv*, a pan-neuronal marker, with TUNEL (Fig. 8L, M) and found several colocalized *elv*$^+$ and TUNEL$^+$ cells at the edge of the epidermis. Our findings suggest that portions of the larval nervous system undergo cell death at metamorphosis and that the nervous system of the anterior ciliary bands may not be maintained in the juvenile body plan as previously proposed [66].

Overall, from our characterization of cell death, we found that an increase in TUNEL$^+$ cells correlated with metamorphosis. We observed TUNEL$^+$ cells broadly distributed in the epidermis and that their restriction over time, from anterior to posterior, correlated with the morphological observation of an anterior to posterior temporal progression of ectodermal thickening [35]**.** While

we cannot rule out additional forms of tissue remodeling or histolysis, our findings suggest that cell death plays an important role in remodeling larval structures specifically in the anterior ciliary bands, which fused during metamorphosis.

Discussion

While the development of an adult by transformation of a larva is very common in bilaterians, we understand very little about the details of how this process occurs at a cellular level, particularly given how the process of metamorphosis differs across groups with different life history strategies [11, 100–102]. This study in the hemichordate *S. californicum* focuses on characterizing the patterns of cellular proliferation and cell death during the two different life history stages and during metamorphosis. Unlike the model species *D. melanogaster*, where metamorphosis results in a major histolysis of larval tissues and the adult emerging from imaginal discs [103], morphological studies in *S. californicum* [35], and indirect developing hemichordates broadly [36], suggest that metamorphosis occurs by remodeling of larval tissues and the transformation of larva into the adult. Our work illustrates the similarities and differences in patterns of proliferation and cell death across distinct life history states in *S. californicum* revealing how and when these unique body plans form.

The larval body plan shaped by proliferation
For an organism with indirect development, rapid growth of the larva is essential. Eggs are small, yet juvenile size at metamorphosis is a good indicator of individual fitness, so larval growth before metamorphosis is critical [13, 104]. We observed in early larval development (Fig. 1B) that the tornaria larva is formed primarily through cell proliferation and limited amounts of cell death (Figs. 2, 3, Additional file 3: S3A–C). The patterns of proliferation we observed highlight regional differences of growth; EdU$^+$ cells were distributed throughout the larval epidermis, the gut, and prominently in the ciliary bands (Figs. 2A, 3A). At this stage in larval development, we observed little cell death with the use of the TUNEL assay (Additional file 3: S3A). There were some TUNEL$^+$ cells distributed throughout the larva, but it does not appear that these cells were concentrated to any structure or tissue. While cell death in bilaterian larval development has not been surveyed broadly across taxa, cell proliferation in larval development has been assessed in a number of marine larvae and the patterns we observe in *S. californicum* confirms and extends what has been found in other species [58].

Origin of the adult body plan begins in the late larva

The morphological discontinuity between larvae and adults has been a consistent source of great curiosity for zoologists [30, 36, 105]. While metamorphosis is often thought of as the time when the adult animal emerges from the vestiges of larval anlage, cell proliferation may precede more overt morphological change at metamorphosis. In the late larva (Fig. 1D) of *S. californicum*, specific regions of the developing adult body are characterized by cell proliferation prior to the organism undergoing the transition from planktonic to benthic during metamorphosis (Fig. 4). At this stage, larvae are competent [9] to begin metamorphosis, but may remain as swimming tornaria for weeks or months. This is most obvious in the proliferation of the coeloms: the protocoel, mesocoel, and metacoel that give rise to the proboscis mesoderm, collar mesoderm, and trunk mesoderm, respectively (Fig. 4H–L). The formation of some of these morphological landmarks prior to metamorphosis has been described previously in *S. californicum* [35] and in enteropneusts broadly [36, 65, 99, 105] but our study clarifies that these structures originate via broad proliferation. Our work describing the patterns of proliferation illustrates the importance of proliferation in the origin of these tissues prior to the start of metamorphosis and supports long-standing hypotheses that the initiation of adult structures before metamorphosis is essential in preparing an organism for a major life history transition [2, 105, 106].

In indirect developing species, questions of adult origins revolve around when and where. The timing of adult formation in the sea urchin *Strongylocentrotus purpuratus* had been described as occurring through "set-aside cells" in which the juvenile grows from a small rudiment within the larval body from a population of sequestered cells [17]. Instead of a cellular identify definition of "set-aside cells", we prefer a broader concept of heterochrony [107, 108] or "deferred development", which focuses on timing of specification and terminal differentiation of some cell populations relative to others [109]. The paradigm of heterochrony or "deferred development" frames the adult development of S. *californicum* as more similar to the delayed life history shift of marine annelids than that of sea urchins [110–112]. In *S. californicum*, we observe this deferral of the adult in the late larva, where proliferation of structures of the adult body plan occurs *prior* to the start of metamorphosis (Fig. 4).

Metamorphosis integrates cell proliferation and cell death

We found that cell death correlated with the onset of metamorphosis, and regionalized cell proliferation that began during late larval development continues into the adult. Cell death was detected in regions, where larval specific structures were remodeled (Fig. 8B, C) and likely is important in shaping the morphogenesis of emerging adult structures, such as the dorsal cord of the forming adult nervous system (Fig. 8E, F, H, I). Clearly the onset of adult morphogenesis, and the initiation of overt metamorphosis, results in a major shift in the patterns of proliferation and cell death.

Cell death within larval-specific structures has long been implicated in studies of metamorphosis, indeed one of the first recorded observation of apoptosis was in the metamorphosis of the toad, *Alytes obstetricans*, in which it was noted that cells of the notochord disappear and are replaced by cells of the vertebrae [113]. Since then, there have been important findings about the role of cell death during anuran metamorphosis that have extended the importance of timing in this process [114–116]. The mechanism of metamorphosis in insects such as butterflies and fruit flies have also provided important comparative perspectives into the role of programmed cell death as a key event in this process [117, 118]. Finally, cell death is implicated in the metamorphosis of marine invertebrates as they transition from planktonic larvae to benthic juveniles [119], in particular in the remodeling of the larval nervous system in gastropods [120, 121]. In *S. californicum* we detected TUNEL$^+$ cells at the start of the morphological metamorphosis, most obviously around the anterior ciliary bands, which were involved in larval feeding, and fuse during metamorphosis (Fig. 8B). This is similar to what has been observed in sea urchins, where apoptotic cells were detected in the arms and ciliary bands of competent larvae [122–124]. Similar to what has been observed in the enteropneust *P. flava* [66], in *S. californicum* the serotonergic neurons associated with ciliary bands are lost at metamorphosis and we observed TUNEL and serotonin double-positive cells suggesting cell death is one way these systems may change at metamorphosis (Fig. 8J, K).

While cell death plays an important role in removing larval-specific structures at metamorphosis, it may also be involved in sculpting larval tissue during metamorphosis, reminiscent of digit development in vertebrates [125], and the formation of leg joints and head segments in *D. melanogaster* [126]. One defining feature of metamorphosis in *S. californicum* is an overall decrease in size that occurs from anterior to posterior. Our finding that cell death proceeds from the anterior to posterior in the dorsal epidermis (Fig. 8E, F) suggest this might be an important process in integrating and removing larval tissue, similar to the apoptosis observed in the mouse paw or fly larva [127]. However, a more complete picture of the type of cell death, apoptosis or necrosis, or programmed cell removal [128] would need to be tested more rigorously with more sophisticated functional

approaches. Overall, while we find that cell death occurs both in larval-specific structures but also broadly in larval tissue during metamorphosis, there are also regions with more limited cell death, such as the anterior ectoderm, collar ectoderm, and tripartite gut, leading to the possibility that not all larval cells die and may instead incorporated into the adult body plan. Our characterization of cell death in *S. californicum* supports classical morphological descriptions that enteropneusts do not have a "catastrophic metamorphosis" [129], and is now confirmed at a cellular level.

Proliferative patterns of growth differ in the adult body plan, as do the markers of these proliferative populations

Juvenile *S. californicum* (Fig. 1J) have distinct patterns of growth—proliferation continues to be enriched in structures that were not functionally part of the larva. The dorsal and ventral cords, gill bars, proboscis ectoderm and lateral groove are all clear examples of regional proliferation of adult structures (Fig. 6B, Additional file 1: S1F). We also looked later in juvenile development and found that proliferation was most striking in the trunk region of the animal that continues to grow (Fig. 6F). This pattern of post-metamorphic growth is reminiscent of the posterior axis elongation by an extended period of posterior growth described in the direct-developing hemichordate *S. kowalevskii* [68].

Given that patterns of cell proliferation differed between larvae and juveniles, we wanted to test whether the genetic signature of proliferative cells was similar or different between the life history states, and if there were specific populations of pluripotent stem cells or broad populations of proliferative progenitors. In organisms such as colonial ascidians [130], acoels [131], flatworms [132, 133], cnidarians [134, 135] and sponges [136], adult stem cells retain the potential to produce both the germline and several somatic cell types, and suggest that there may be an ancestral animal stem cell [137]. We did not recover a clear pluripotent stem cell population, in contrast to organisms with clear neoblast populations, such as platyhelminthes and acoels [71]. Genes associated with multipotency or germline multipotency also did not have significant differential expression (Additional file 4: S4C, S4D). Instead, we found differential expression of genes, such as *lbr-1* in both larvae and juveniles, pointing towards the importance of chromatin state independent of the type of proliferative cell. It was previously suggested that the patterns of *lbr* and *lamA/C* expression in a number of different mammalian cell types may be indicative of peripheral heterochromatin tethers regulating differentiation and perhaps this is a larger uniting trend across deuterostomes [91].

When we looked at the differential expression in irradiated vs. non-irradiated larvae, we found a relatively limited number of significantly differentially expressed genes, such as those involved in cell division (such as *ince, asmp-1, dlgp5*) and most interestingly *fgfr-B* (fibroblast growth factor receptor B). A similar approach in the parasite *Schistosoma mansoni* found FGF receptors were downregulated in response to irradiation, and further showed that the inhibition of FGF signaling with RNAi resulted in reduced EdU incorporation and down regulation of cell-cycle-associated transcripts [138]. In juvenile animals, while we did recover the expression of what may be a germline specific marker in *spindle-E*, there were also a number of transcripts from our irradiation experiment that suggest a potential immune response, such as *traf2*, *tlr2* and *tlr6*. We conclude that the differential expression of these genes is likely related less to the depletion of irradiation-sensitive transcripts and more likely an immune reaction in response to the irradiation.

While additional work will need to be done to determine if markers, such as *fgr-B* and *spindle-E* are lineage and life history-specific proliferation markers, our results certainly support the hypothesis that formation of larval and juvenile structures draws on distinct sets of proliferative populations. The strong focus on species with direct development may miss some interesting regulatory features of distinct proliferative cell populations related to the development of complex life cycles. For a fuller understanding of developmental diversity and how it has shaped animal body plans, we need both a broader phylogenetic sampling but also greater representation of complex developmental strategies.

Integration of larval and adult body plans

Our study of the balance and timing between cell proliferation and cell death illustrates that adult morphological elements proliferate prior to the start of metamorphosis, and that the onset of metamorphosis correlates with the onset of cell death. However, this study has also raised more questions, particularly the mysterious fate of most larval cells that are seemingly maintained through the threshold of metamorphosis. The most provocative and exciting possibility is the potential of larval cells taking on new identities in the adult body plan. In sea urchins, which were the key example of catastrophic metamorphosis with set-aside cells, the organization of the larval epithelium is preserved as regionalized apoptosis occurs in the larval arms that are resorbed [124]. Morphological studies of other echinoderms such as sea cucumbers and cidaroids suggest that much of their larval epidermis is maintained into the juvenile stage and is not lost at metamorphosis [139, 140]. Even in examples, such as nemerteans, which are described as "maximally-indirect

developers" [141], we now know that the cells that create the imaginal discs also contribute to the larval body [142]. Even in *D. melanogaster* with its specialized imaginal disc cells, differentiated larval tracheal cells become proliferative and form the adult trachea and also adult-specific air sacs [143, 144]. In the tobacco hornworm, *Manduca sexta,* differentiated cells of the larval legs contribute to the adult legs [145]. Perhaps this linkage between larval and adult cells is quite common. While genetic tools would need to be developed to study this in detail, studies of transformational metamorphosis have the potential test whether transdifferentiation of cell types occurs as part of normal ontological development in organisms with complex life histories. If this is indeed true, we are left with a tantalizing question, when many larval cells remain, how do they take on the appropriate function in the adult?

Almost all our understanding of adult development comes from direct developers, where the adult body plan emerges from the embryo. Despite the prevalence and phylogenetic breadth of species that represent indirect development, we understand very little about how adult development occurs by transformation. Clearly a greater focus is needed on the range of development strategies that characterize metamorphosis in metazoans. Only through this broader sampling of life history strategies can we hope for a more comprehensive understanding of the developmental mechanisms responsible for adult body plan formation.

Conclusions
Our study describes cell proliferation and cell death through the development of the indirect developing *S. californicum*. This species has distinct larval and adult body plans and like other indirect-developing hemichordates [31, 33, 98] a metamorphosis that is more transformational than catastrophic. Our data represent a cellular investigation into the common, yet understudied, bilaterian developmental strategy of formation of adult body plan by transformation of a larval body plan. Despite the prevalence of this life history strategy, we have little developmental insights into how this process occurs. Our study uncovered that the broad proliferation of adult body plan components starts prior to any overt metamorphosis. Although cell death was a prominent feature of metamorphosis and adult body plan development, it is unlikely that the entire cell complement of the adult can be explained by larval cell death and proliferation of a distinct adult stem cell population. Future studies will be needed to clarify the fate of larval cells through metamorphosis. Altogether, our study establishes a cellular characterization of the formation of larval and adult body plans and transitions through metamorphosis in *S.* *californicum,* an important species for understanding this transformational process through the lens of cell, developmental, and evolutionary biology.

Methods
Collecting, spawning, and larval rearing
Adult *Schizocardium californicum* were collected in Morro Bay State Park, California, in a mudflat located at 35°20′56.7″N 120°50′35.6″W with appropriate state permitting. Animals were spawned as described in [35] with individual females transferred in bowls of filtered seawater and placed in an illuminated incubator at 24–26 °C. Once hatched, larvae were transferred to 1 gallon glass jars with continuous stirring and fed larvae with a 1:1 mix of *Dunaliella tertiolecta* and *Rhodomonas lens*. Every two to four days, containers are washed, water was replaced with clean filtered seawater, and fresh algae was added. To grow larger numbers of animals, some larvae were placed on a continuous flow-through system by being transferred into diffusion tubes [146]. Once animals began metamorphosis, they were transferred into glass bowls with terrarium sand.

EdU labeling
Labeling and detection of proliferating cells were performed using the Click-it Plus EdU 488 Imaging Kit (Life Technologies), with the following modifications. Larva and juvenile worms were cultured in FSW supplemented with 10 µM EdU diluted from a 10 mM stock in DMSO. Unless otherwise noted, animals were pulsed for 30 min with EdU then fixed with 3.7% paraformaldehyde in MOPS fix buffer (0.1 M MOPS, 0.5 M NaCl, 2 mM EGTA, 1 mM MgCl2, 1× PBS) for 1 h at room temperature (RT). For detection of EdU incorporation, labeled embryos were transferred to a solution of PBS and the detection was performed following the manufacturer's protocol with an increased permeabilization time in 0.5% Triton® X-100 in PBS of 40 min and an increased detection time of 45 min.

TUNEL detection
Detection of apoptotic cells were performed using the Click-iT Plus TUNEL Assay for in situ apoptosis detection with Alexa FluorTM dyes, with the following modifications. Animals were fixed with the standard protocol (3.7% paraformaldehyde in MOPS fix buffer), washed twice in 1 × PBS and permeabilized with proteinase-K for 15 min at room temperature. TdT reaction mixture was incubated for 60 min at 37 °C and Click-iT Plus reaction was carried out for 30 min at 37 °C.

Antibody labeling

Fixation and antibody labeling was performed as described previously [35]. To visualize proliferative cells, we used a rabbit polyclonal anti-histone H3 (phospho S10) (Abcam ab5176) diluted 1:200 in blocking solution. To visualize cilia, we used a mouse monoclonal anti-acetylated tubulin antibody (Sigma T7451) diluted 1:400 in blocking solution. To visualize the serotonergic nervous system, we used a rabbit anti-serotonin antibody (Sigma S5545) diluted 1:300 in blocking solution. Secondary antibodies (ThermoFisher, Alexa Fluor) were added at 1:1000 dilution to the blocking solution.

Imaging

Nuclei were stained with Hoechst 33,342 (1:1000) in PBS and mounted in PBS using coverslips elevated with clay feet. For juvenile worms, samples were transferred into 50% glycerol for 30–60 min, then 70% glycerol for imaging. Samples were imaged on a Zeiss LSM 700 with 10X, 20X and $40\times$ objectives. For samples larger than the field of view, maximal intensity projections from several stacks were stitched together (Fiji).

Irradiation and transcriptional profiling

Larva and juvenile worms were exposed to 120 and 200 Gy of X-ray irradiation on a CellRad Faxitron source. Animals were cultured in FSW after irradiation for 3 days and purified total RNA was prepared from pools of 5 animals using Qiagen RNeasy. Three independent biological replicates were performed for both control and irradiated experimental groups. Individually tagged libraries for RNA-seq were prepared (Nugen-Tecan Genomics Universal mRNA-seq Kit), pooled in a single lane, and 75-bp pair-reads were generated using an Illumina HiSeq2000 at the Chan-Zuckerberg Biohub. The resulting reads were mapped to the annotated *S. californicum* genome (v2.0) using CLC Genomics Workbench (CLC Bio) and differential expression was conducted with DeSeq2. *apeglm* was used for log fold change shrinkage [147] and *v*st (variance stabilizing transformation) was used for visualization [148].

In-situ hybridization

Samples were relaxed using 3.5% MgCl2 prior to fixation and fixed in 3.7% formaldehyde in MOPS fix buffer for 1 h at room temperature (RT), washed in fix buffer, dehydrated in 100% ethanol and stored at − 20 °C. Genes were amplified from stage specific cDNA with random hexamers and cloned into pGEM-T Easy (Promega). Digoxygenin labeled antisense probes were synthesized using SP6 or T7 RNA polymerase (Promega). In situ hybridization was performed a combination of what has been described previously [52, 149]. RNA probes were diluted to 0.1–1 ng/ml and hybridized overnight at 60 °C and visualized using an Anti-DIG AP antibody and TSA-Cy3.

In situ HCR version 3.0.

Complementary DNA sequences specific to genes of interest were submitted to the in situ probe generator from the Ozpolat Lab [150]. Gene orthology was determined by collecting sequences of interest from related species and then building gene trees. Sequences were aligned with MUSCLE [151] and trees were calculated with Bayesian inference trees using MrBayes version 3.1.2 [152] in 1,000,000 generations with sampling of trees every 100 generations and a burn-in period of 25% (Additional file 4: S4). The sequences generated by the software were used to order DNA oligo pools (50 μmol DNA oPools Oligo Pool) from Integrated DNA Technologies, resuspended to 1 μmol/μl in 50 mM Tris buffer, pH 7.5. HCR amplifiers with fluorophores B1-Alexa Fluor-546, B2-Alexa Fluor-488, and B3-Alexa Fluor-647 were ordered from Molecular Instruments, Inc. The HCR was performed based on Choi et al., 2018 and the Hybridization Chain Reaction (HCR) In Situ Protocol from the Patel Lab [153, 154]. For experiments that involved HCR and TUNEL labeling, HCR was conducted first, and then additional labeling was performed after.

Supplementary Information

The online version contains supplementary material available at https://doi.org/10.1186/s13227-022-00198-1.

Additional file 1: S1. Additional characterization of proliferative cells in *S. californicum*. A) Bar chart of number of Hoesch + in the ciliary bands vs. non ciliary bands, error bars are ± 1 SD (66% Confidence interval). B) Bar chart of EdU + cells in the ciliary bands vs. non ciliary bands, error bars are ± 1 SD (66% Confidence interval). C–F) All: anterior up; scale bar is 100um. blue = Hoechst, green = EdU. C) Ventral view of EdU distribution early in metamorphosis. D) Ventral view of EdU distribution in the middle of metamorphosis. E) Lateral view of EdU distribution at the end of metamorphosis. F) Ventral view of EdU distribution in juveniles. G–H) Expression of h2b mRNA and EdU positive cells in the juvenile proboscis blue = Hoechst, yellow = h2b mRNA, green = EdU.

Additional file 2: S2. Differential expression of larval and juvenile transcriptomes, irradiated versus non-irradiated. A) Differential expression of larval transcriptomes with baseMean, log2FoldChange, lfcSE, pvalue, padj. B) Differential expression of juvenile transcriptomes with baseMean, log2FoldChange, lfcSE, pvalue, padj. C) Differential expression of *piwi, vasa,* and *nanos* in larvae with baseMean, log2FoldChange, lfcSE, pvalue, padj. D) Differential expression of *piwi, vasa,* and *nanos* in juveniles with baseMean, log2FoldChange, lfcSE, pvalue, padj.

Additional file 3: S3. Additional characterization of TUNEL during larval development and metamorphosis. All: blue = Hoechst, grey = TUNEL, scale bar is 100um. A) lateral of view of mid tornaria body plan. B) Late larva with very few TUNEL + cells. C, Highlights regions of B) a few TUNEL + cells. C). D) Early in metamorphosis from Fig. 7C with an increase in TUNEL + cells. E) TUNEL + cells found in the mesodermal protocoel. F) Ventral view during the middle of metamorphosis. G) Positive control of TUNEL labeling by artificially nicking the ends of DNA with DNAse-1

metamorphosis H) Inset of positive control with TUNEL detected in deeper tissue layers

Additional file 4: S4. Gene Trees of HCR candidate Genes. Gene trees for A) Lbr-1 B) Fgfr C) Spne-2

Availability of data and materials

Sequencing raw reads and processed counts matrices associated with this study are available in the NCBI Gene Expression Omnibus (GEO), https://www.ncbi.nlm.nih.gov/geo/query/acc.cgi?acc=GSE196326.

Declarations

Ethics approval and consent to participate
Not applicable.

Consent for publication
Not applicable.

Competing interests
Not applicable.

Author details
[1]Hopkins Marine Station, Department of Biology, Stanford University, Pacific Grove, CA, USA. [2]Department of Bioengineering, Stanford University, Stanford, CA, USA. [3]California State University of Monterey Bay, Monterey, CA, USA. [4]CZ Biohub, San Francisco, CA, USA.

References

1. Cameron CB, Perez M. Spengelidae (Hemichordate: Enteropnuesta) from the Eastern Pacific including a new species, *Schizocardium californicum*, from California. Zootaxa. 2012;3569:79–88.
2. Jäegersten G. Evolution of the metazoan life cycle; a comprehensive theory. New York: Academic Press; 1972.
3. Nielsen C, Nørrevang A. The trochaea theory: an example of life cycle phylogeny. In: Conway Morris S, George JD, Gibson R, Platt HM, editors. The origins and relationships of lower invertebrates, vol. The systematics association special volume; 28. Oxford: Oxford University Press; 1985. p. 28–41.
4. Raff RA. Origins of metazoan body plans: the larval revolution. Anim Evol. 2009;43:1473–9.
5. Hyman LH. The invertebrates, vol. 4. New York: McGraw-Hill; 1955.
6. Nielsen C. Animal evolution: interrelationships of the living Phyla. 3rd ed. Oxford: Oxford University Press; 2012.
7. Gilbert L, Frieden E, editors. Metamorphosis, a problem in developmental biology. 2nd ed. New York: Plenum Press; 1981.
8. McEdward LR, Janies DA. Life cycle evolution in asteroids: what is a larva? Biol Bull. 1993;184(3):255–68.
9. Hadfield MG, Carpizo-Ituarte EJ, del Carmen K, Nedved BT. Metamorphic competence, a major adaptive convergence in marine invertebrate larvae. Am Zool. 2001;41(5):1123–31.
10. Strathmann RR. Hypotheses on the origins of marine larvae. Annu Rev Ecol Syst. 1993;24(1):89–117.
11. Bishop CD, Erezyilmaz DF, Flatt T, Georgiou CD, Hadfield MG, Heyland A, et al. What is metamorphosis? Integr Comp Biol. 2006;46(6):655–61.
12. Emlet RB. Echinoderm larval ecology viewed from the egg. Echinoderm Stud. 1987;2:55–136.
13. Strathmann RR. Feeding and nonfeeding larval development and life-history evolution in marine invertebrates. Annu Rev Ecol Syst. 1985;16(1):339–61.
14. Damen P, Dictus WJ. Cell lineage of the prototroch of *Patella vulgata* (Gastropoda, Mollusca). Dev Biol. 1994;162(2):364–83.
15. Page LR. Molluscan larvae: pelagic juveniles or slowly metamorphosing larvae? Biol Bull. 2009;216(3):216–25.
16. Okazaki K. Normal development to metamorphosis. In: Czihak G, editor. The sea Urchin Embryo. Berlin: Springer; 1975. p. 177–232.
17. Peterson KJ, Cameron RA, Davidson EH. Set-aside cells in maximal indirect development: evolutionary and developmental significance. BioEssays. 1997;19(7):623–31.
18. Maslakova SA. Development to metamorphosis of the nemertean pilidium larva. Front Zool. 2010;7(1):30.
19. Nielsen C. Trochophora larvae: cell-lineages, ciliary bands, and body regions. 1. Annelida and Mollusca. J Exp Zool. 2004;302B(1):35–68.
20. van der Horst CJ. Hemichordata. In: Klassen und Ordnungen des Tierreichs wissenschaftlich dargestellt. Akademische Verlag; 1939. (Wort und Bild; vol. 4).
21. Hyman LH. The invertebrates: smaller coelomate groups, Chaetognatha, Hemichordata, Pogonophora, Phoronida, Ectoprocta, Brachipoda, Sipunculida, the coelomate Bilateria, vol. 5. New York: McGraw-Hill; 1959.
22. Cameron CB. A phylogeny of the hemichordates based on morphological characters. Can J Zool. 2005;83(1):196–215.
23. Cannon JT, Rychel AL, Eccleston H, Halanych KM, Swalla BJ. Molecular phylogeny of hemichordata, with updated status of deep-sea enteropneusts. Mol Phylogenet Evol. 2009;52(1):17–24.
24. Bromham LD, Degnan BM. Hemichordates and deuterostome evolution: robust molecular phylogenetic support for a hemichordate + echinoderm clade. Evol Dev. 1999;1(3):166–71.
25. Cameron CB, Garey JR, Swalla BJ. Evolution of the chordate body plan: New insights from phylogenetic analyses of deuterostome phyla. Proc Natl Acad Sci. 2000;97(9):4469–74.
26. Furlong RF, Holland PH. Bayesian phylogenetic analysis supports monophyly of Ambulacraria and of cyclostomes. Zool Sci. 2002;19(5):593–9.
27. Cannon JT, Kocot KM, Waits DS, Weese DA, Swalla BJ, Santos SR, et al. Phylogenomic resolution of the hemichordate and echinoderm clade. Curr Biol. 2014;24(23):2827–32.
28. Kapli P, Natsidis P, Leite DJ, Fursman M, Jeffrie N, Rahman IA, et al. Lack of support for deuterostomia prompts reinterpretation of the first bilateria. Sci Adv. 2021. https://doi.org/10.1126/sciadv.abe2741.
29. Morgan TH. The development of Balanoglossus. J Morphol. 1894;9(1):1–86.
30. Agassiz A. The History of Balanoglossus and Tornaria. Mem Am Acad Arts Sci. 1873;9(2):421–36.

31. Lin CY, Tung CH, Yu JK, Su YH. Reproductive periodicity, spawning induction, and larval metamorphosis of the hemichordate acorn worm *Ptychodera flava*: Animal Resources for the Acorn Worm *Ptychodera Flava*. J Exp Zool B Mol Dev Evol. 2016;326(1):47–60.

32. Hadfield MG. Hemichordata. In: Reproduction of Marine Invertebrates [Internet]. Elsevier; 1975 [cited 2022 Mar 29]. p. 185–240. https://linki nghub.elsevier.com/retrieve/pii/B9780122825026500121.

33. Urata M, Yamaguchi M. The development of the enteropneust hemichordate *Balanoglossus misakiensis* Kuwano. Zool Sci. 2004;21(5):533–40.

34. Miyamoto N, Saito Y. Morphology and development of a new species of Balanoglossus (Hemichordata: Enteropneusta: Ptychoderidae) from Shimoda, Japan. Zool Sci. 2007;24(12):1278–85.

35. Gonzalez P, Jiang JZ, Lowe CJ. The development and metamorphosis of the indirect developing acorn worm *Schizocardium californicum* (Enteropneusta: Spengelidae). Front Zool. 2018. https://doi.org/10.1186/s12983-018-0270-0.

36. Morgan TH. The growth and metamorphosis of Tornaria. J Morphol. 1891;5:407–58.

37. Harada Y, Okai N, Taguchi S, Tagawa K, Humphreys T, Satoh N. Developmental expression of the hemichordate otx ortholog. Mech Dev. 2000;91(1–2):337–9.

38. Harada Y, Okai N, Taguchi S, Shoguchi E, Tagawa K, Humphreys T, et al. Embryonic Expression of a Hemichordate distal-less Gene. Zool Sci. 2001;18(1):57–61.

39. Harada Y, Shoguchi E, Taguchi S, Okai N, Humphreys T, Tagawa K, et al. Conserved expression pattern of BMP-2/4 in hemichordate acorn worm and echinoderm sea cucumber embryos. Zool Sci. 2002;19(10):1113–21.

40. Ogasawara M, Wada H, Peters H, Satoh N. Developmental expression of Pax1/9 genes in urochordate and hemichordate gills: insight into function and evolution of the pharyngeal epithelium. Dev Camb Engl. 1999;126(11):2539–50.

41. Okai N, Tagawa K, Humphreys T, Satoh N, Ogasawara M. Characterization of gill-specific genes of the acorn worm *Ptychodera flava*. Dev Dyn. 2000;217(3):309–19.

42. Peterson KJ, Cameron RA, Tagawa K, Satoh N, Davidson EH. A comparative molecular approach to mesodermal patterning in basal deuterostomes: the expression pattern of Brachyury in the enteropneust hemichordate *Ptychodera flava*. Development. 1999;126(1):85–95.

43. Tagawa K, Humphreys T, Satoh N. Novel pattern of Brachyury gene expression in hemichordate embryos. Mech Dev. 1998;75(1–2):139–43.

44. Tagawa K, Humphreys T, Satoh N. T-brain expression in the apical organ of hemichordate tornaria larvae suggests its evolutionary link to the vertebrate forebrain. J Exp Zool. 2000;31:23–31.

45. Tagawa K, Satoh N, Humphreys T. Molecular studies of hemichordate development: a key to understanding the evolution of bilateral animals and chordates. Evol Dev. 2001;3(6):443–54.

46. Taguchi S, Tagawa K, Humphreys T, Nishino A, Satoh N, Harada Y. Characterization of a hemichordate fork head/HNF-3 gene expression. Dev Genes Evol. 2000;210(1):11–7.

47. Taguchi S, Tagawa K, Humphreys T, Satoh N. Group B sox genes that contribute to specification of the vertebrate brain are expressed in the apical organ and ciliary bands of hemichordate larvae. Zool Sci. 2002;19(1):57–66.

48. Takacs CM, Moy VN, Peterson KJ. Testing putative hemichordate homologues of the chordate dorsal nervous system and endostyle: expression of NK2.1 (TTF-1) in the acorn worm *Ptychodera flava* (Hemichordata, Ptychoderidae). Evol Dev. 2002;4(6):405–17.

49. Röttinger E, Martindale MQ. Ventralization of an indirect developing hemichordate by NiCl2 suggests a conserved mechanism of dorso-ventral (D/V) patterning in Ambulacraria (hemichordates and echinoderms). Dev Biol. 2011;354(1):173–90.

50. Röttinger E, DuBuc TQ, Amiel AR, Martindale MQ. Nodal signaling is required for mesodermal and ventral but not for dorsal fates in the indirect developing hemichordate *Ptychodera flava*. Biol Open. 2015;4(7):830–42.

51. Kaul-Strehlow S, Urata M, Praher D, Wanninger A. Neuronal patterning of the tubular collar cord is highly conserved among enteropneusts but dissimilar to the chordate neural tube. Sci Rep. 2017;7(1):7003.

52. Gonzalez P, Uhlinger KR, Lowe CJ. The adult body plan of indirect developing hemichordates develops by adding a hox-patterned trunk to an anterior larval territory. Curr Biol. 2016;27(1):1–9.

53. Fan TP, Ting HC, Yu JK, Su YH. Reiterative use of FGF signaling in mesoderm development during embryogenesis and metamorphosis in the hemichordate *Ptychodera flava*. BMC Evol Biol. 2018;18(1):120.

54. Salic A, Mitchison TJ. A chemical method for fast and sensitive detection of DNA synthesis in vivo. Proc Natl Acad Sci. 2008;105(7):2415.

55. Garstang W. Spolia Bermudiana. II. The ciliary feeding mechanism of Tornaria. J Cell Sci. 1939;81:347–66.

56. Lacalli TC, Gilmour THJ. Locomotory and feeding effectors of the tornaria larva of *Balanoglossus biminiensis*: Tornaria structure and feeding. Acta Zool. 2002;82(2):117–26.

57. Strathmann R, Bonar D. Ciliary feeding of tornaria larvae of *Ptychodera flava* (Hemichordata: Enteropneusta). Mar Biol. 1976;34(4):317–24.

58. Bird A. Comparative analysis of cell proliferation patterns in ciliated planktotrophic larvae of marine invertebrates (Master of Science). University of Oregon; 2012.

59. Lacalli TC. Apical organs, epithelial domains, and the origin of the chordate central nervous system. Am Zool. 1994;34(4):533–41.

60. Marlow H, Tosches MA, Tomer R, Steinmetz PR, Lauri A, Larsson T, et al. Larval body patterning and apical organs are conserved in animal evolution. BMC Biol. 2014;12(1):7.

61. Nakajima Y, Humphreys T, Kaneko H, Tagawa K. Development and Neural Organization of the Tornaria Larva of the Hawaiian Hemichordate, *Ptychodera flava*. Zool Sci. 2004;21(1):69–78.

62. Nielsen C. Larval and adult brains. Evol Dev. 2005;7(5):483–9.

63. Ruppert EE, Balser EJ. Nephridia in the larvae of hemichordates and echinoderms. Biol Bull. 1986;171(1):188–96.

64. Gąsiorowski L, Andrikou C, Janssen R, Bump P, Budd GE, Lowe CJ, et al. Molecular evidence for a single origin of ultrafiltration-based excretory organs. Curr Biol. 2021;31(16):3629-3638.e2.

65. Gilmour THJ. Feeding in tornaria larvae and the development of gill slits in enteropneust hemichordates. Can J Zool. 1982;60(12):3010–20.

66. Nielsen C, Hay-Schmidt A. Development of the enteropneust *Ptychodera flava*: ciliary bands and nervous system. J Morphol. 2007;268(7):551–70.

67. Gillis JA, Fritzenwanker JH, Lowe CJ. A stem-deuterostome origin of the vertebrate pharyngeal transcriptional network. Proc R Soc B Biol Sci. 2012;279(1727):237–46.

68. Fritzenwanker JH, Uhlinger KR, Gerhart J, Silva E, Lowe CJ. Untangling posterior growth and segmentation by analyzing mechanisms of axis elongation in hemichordates. Proc Natl Acad Sci. 2019;116(17):8403–8.

69. Bardeen CR, Baetjer FH. The inhibitive action of the Roentgen rays on regeneration in planarians. J Exp Zool. 1904;1(1):191–5.

70. Till JE, McCulloch EA. A direct measurement of the radiation sensitivity of normal mouse bone marrow cells. Radiat Res. 1961;14(2):213–22.

71. Eisenhoffer GT, Kang H, Alvarado AS. Molecular analysis of stem cells and their descendants during cell turnover and regeneration in the planarian *Schmidtea mediterranea*. Cell Stem Cell. 2008;3(3):327–39.

72. Solana J, Kao D, Mihaylova Y, Jaber-Hijazi F, Malla S, Wilson R, et al. Defining the molecular profile of planarian pluripotent stem cells using a combinatorial RNA-seq, RNA interference and irradiation approach. Genome Biol. 2012;13(3):R19.

73. Wagner DE, Ho JJ, Reddien PW. Genetic regulators of a pluripotent adult stem cell system in planarians identified by RNAi and clonal analysis. Cell Stem Cell. 2012;10(3):299–311.

74. Newmark PA, Sánchez AA. Bromodeoxyuridine specifically labels the regenerative stem cells of planarians. Dev Biol. 2000;220(2):142–53.

75. Baguña J, Auladell C. Regeneration and pattern formation in planarians III. Evidence that neoblasts are totipotent stem cells and the source of blastema cells. Development. 1989;86:77–86.

76. Juliano CE, Swartz SZ, Wessel GM. A conserved germline multipotency program. Development. 2010;137(24):4113–26.

77. Earnshaw WC, Cooke CA. Analysis of the distribution of the INCENPs throughout mitosis reveals the existence of a pathway of structural changes in the chromosomes during metaphase and early events in cleavage furrow formation. J Cell Sci. 1991;98(4):443–61.

78. Fish JL, Kosodo Y, Enard W, Paabo S, Huttner WB. Aspm specifically maintains symmetric proliferative divisions of neuroepithelial cells. Proc Natl Acad Sci. 2006;103(27):10438–43.

79. Gonzalez C, Saunders RDC, Casal J, Carmena M, Ripoll P, Glover DM. Mutations at the *asp* locus of *Drosophila* lead to multiple free centrosomes in syncytial embryos, but restrict centrosome duplication in larval neuroblasts. J Cell Sci. 1990. https://doi.org/10.1242/jcs.96.4.605.

80. Ripoll P, Pimpinelli S, Valdivia MM, Avila J. A cell division mutant of *Drosophila* with a functionally abnormal spindle. Cell. 1985;41(3):907–12.

81. Stewart M, Murphy C, Fristrom JW. The recovery and preliminary characterization of x chromosome mutants affecting imaginal discs of *Drosophila melanogaster*. Dev Biol. 1972. https://doi.org/10.1016/0012-1606(72)90113-3.

82. Woods DF, Bryant PJ. The discs-large tumor suppressor gene of *Drosophila* encodes a guanylate kinase homolog localized at septate junctions. Cell. 1991;66(3):451–64.

83. Vanden Bosch A, Raemaekers T, Denayer S, Torrekens S, Smets N, Moermans K, et al. NuSAP is essential for chromatin-induced spindle formation during early embryogenesis. J Cell Sci. 2010;123(19):3244–55.

84. Chiquet-Ehrismann R, Orend G, Chiquet M, Tucker RP, Midwood KS. Tenascins in stem cell niches. Matrix Biol. 2014;37:112–23.

85. Lanner F, Rossant J. The role of FGF/Erk signaling in pluripotent cells. Development. 2010;137(20):3351–60.

86. Rebscher N, Deichmann C, Sudhop S, Fritzenwanker JH, Green S, Hassel M. Conserved intron positions in FGFR genes reflect the modular structure of FGFR and reveal stepwise addition of domains to an already complex ancestral FGFR. Dev Genes Evol. 2009;219(9–10):455–68.

87. Green SA, Norris RP, Terasaki M, Lowe CJ. FGF signaling induces mesoderm in the hemichordate *Saccoglossus kowalevskii*. Development. 2013;140(5):1024–33.

88. Malone CD, Brennecke J, Dus M, Stark A, McCombie WR, Sachidanandam R, et al. Specialized piRNA pathways act in germline and somatic tissues of the *Drosophila* ovary. Cell. 2009;137(3):522–35.

89. Ott KM, Nguyen T, Navarro C. The DExH box helicase domain of spindle-E Is necessary for retrotransposon silencing and axial patterning during *Drosophila* oogenesis. G3. 2014;4(11):2247–57.

90. Lin C, Yu J, Su Y. Evidence for BMP-mediated specification of primordial germ cells in an indirect-developing hemichordate. Evol Dev. 2021;23(1):28–45.

91. Solovei I, Wang AS, Thanisch K, Schmidt CS, Krebs S, Zwerger M, et al. LBR and Lamin A/C sequentially tether peripheral heterochromatin and inversely regulate differentiation. Cell. 2013;152(3):584–98.

92. Olins AL, Rhodes G, Welch DBM, Zwerger M, Olins DE. Lamin B receptor: multi-tasking at the nuclear envelope. Nucleus. 2010;1(1):53–70.

93. Gavrieli Y, Sherman Y, Ben-Sasson SA. Identification of programmed cell death in situ via specific labeling of nuclear DNA fragmentation. J Cell Biol. 1992;119(3):493–501.

94. Ansari B, Coates PJ, Greenstein BD, Hall PA. In situ end-labelling detects DNA strand breaks in apoptosis and other physiological and pathological states. J Pathol. 1993;170(1):1–8.

95. Charriaut-Marlangue C, Ben-Ari Y. A cautionary note on the use of the TUNEL stain to determine apoptosis. NeuroReport. 1995;7(1):61–4.

96. Kolb HC, Finn MG, Sharpless KB. Click chemistry: diverse chemical function from a few good reactions. Angew Chem Int Ed. 2001;40(11):2004–21.

97. Rostovtsev VV, Green LG, Fokin VV, Sharpless KB. A stepwise huisgen cycloaddition process: copper(I)-catalyzed regioselective "ligation" of azides and terminal alkynes. Angew Chem Int Ed. 2002;41(14):2596–9.

98. Miyamoto N, Nakajima Y, Wada H, Saito Y. Development of the nervous system in the acorn worm *Balanoglossus simodensis*: insights into nervous system evolution: development of hemichordate nervous system. Evol Dev. 2010;12(4):416–24.

99. Kaul-Strehlow S, Urata M, Minokawa T, Stach T, Wanninger A. Neurogenesis in directly and indirectly developing enteropneusts: of nets and cords. Org Divers Evol. 2015;15(2):405–22.

100. Strathmann MF. Reproduction and development of marine invertebrates of the northern Pacific coast: data and methods for the study of eggs, embryos, and larvae. Seattle: University of Washington Press; 1987.

101. Giese AC. Reproduction of marine invertebrates. New York: Academic Press; 1974.

102. Grant PT, Mackie AM, editors. Chemoreception in marine organisms. London: Academic Press; 1974.

103. Wigglesworth VB. Insect physiology. 7th ed. New York: Springer; 2013.

104. Hadfield MG. Why and how marine-invertebrate larvae metamorphose so fast. Semin Cell Dev Biol. 2000;11(6):437–43.

105. Ritter WE. On a new balanoglossus larva from the coast of california, and its possession of an endostyle. Zool Anz. 1894;17:24–60.

106. Mortensen T. Studies of the development and larval forms of echinoderms. Copenhagen: Bianco Lunos; 1921. p. 261.

107. Marlow H. Evolutionary development of marine larvae. In: Carrier T, Reitzel A, Heyland A, editors. Evolutionary ecology of marine invertebrate larvae. Oxford: Oxford University Press; 2017.

108. Brambell FWR, Cole HA. The preoral ciliary organ of the enteropneusta: its occurrence, structure, and possible phylogenetic significance. Proc Zool Soc Lond. 1939;B109(2):181–93.

109. Bishop C, Hall B. Deferring development: setting aside cells for future use in development and evolution. Boca Raton: CRC Press/Taylor & Francis Group; 2020.

110. Seaver EC, Thamm K, Hill SD. Growth patterns during segmentation in the two polychaete annelids, *Capitella sp.* and *Hydroides elegans*: comparisons at distinct life history stages. Evol Dev. 2005;7(4):312–26.

111. Strathmann RR. Functional design in the evolution of embryos and larvae. Semin Cell Dev Biol. 2000;11(6):395–402.

112. Arenas-Mena C. Indirect development, transdifferentiation and the macroregulatory evolution of metazoans. Philos Trans R Soc B Biol Sci. 2010;365(1540):653–69.

113. Vogt KC. Untersuchungen Über Die Entwicklungsgeschichte der Geburtshelferkröte (*Alytes Obstetricans*). 1842.

114. Estabel J, Mercer A, König N, Exbrayat J-M. Programmed cell death in *Xenopus laevis* spinal cord, tail and other tissues, prior to, and during, metamorphosis. Life Sci. 2003;73(25):3297–306.

115. Okada M, Miller TC, Wen L, Shi YB. A balance of Mad and Myc expression dictates larval cell apoptosis and adult stem cell development during *Xenopus* intestinal metamorphosis. Cell Death Dis. 2017;8(5):e2787–810.

116. Ishizuya-Oka A, Shi Y-B. Regulation of adult intestinal epithelial stem cell development by thyroid hormone during *Xenopus laevis* metamorphosis. Dev Dyn. 2007;236(12):3358–68.

117. Meuser S, Pflüger H-J. Programmed cell death specifically eliminates one part of a locust pleuroaxillary muscle after the imaginal moult. J Exp Biol. 1998;201:2367–82.

118. Tettamanti G, Casartelli M. Cell death during complete metamorphosis. Philos Trans R Soc B Biol Sci. 2019;374(1783):20190065.

119. Wynen H, Heyland A. Hormonal Regulation of Programmed Cell Death in Sea Urchin Metamorphosis. Front Ecol Evol. 2021;8(9): 733787.

120. Leise EM, Kempf SC, Durham NR, Gifondorwa DJ. Induction of metamorphosis in the marine gastropod *Ilyanassa obsoleta*: 5HT, NO and programmed cell death. Acta Biol Hung. 2004;55(1–4):293–300.

121. Kiss T. Apoptosis and its functional significance in molluscs. Apoptosis. 2010;15(3):313–21.

122. Roccheri MC, Tipa C, Bonaventura R, Matranga V. Physiological and induced apoptosis in sea urchin larvae undergoing metamorphosis. Int J Dev Biol. 2002;46:801–6.

123. Lutek K, Dhaliwal RS, Van Raay TJ, Heyland A. Sea urchin histamine receptor 1 regulates programmed cell death in larval *Strongylocentrotus purpuratus*. Sci Rep. 2018;8(1):4002.

124. Sato Y, Kaneko H, Negishi S, Yazaki I. Larval arm resorption proceeds concomitantly with programmed cell death during metamorphosis of the sea urchin *Hemicentrotus pulcherrimus*. Cell Tissue Res. 2006;326(3):851–60.

125. Lindsten T, Ross AJ, King A, Zong W-X, Rathmell JC, Shiels HA, et al. The combined functions of proapoptotic Bcl-2 family members Bak and Bax are essential for normal development of multiple tissues. Mol Cell. 2000;6(6):1389–99.

126. Lohmann I, McGinnis N, Bodmer M, McGinnis W. The *Drosophila Hox* gene deformed sculpts head morphology via direct regulation of the apoptosis activator *reaper*. Cell. 2002;110(4):457–66.

127. Fuchs Y, Steller H. Programmed cell death in animal development and disease. Cell. 2015;147(4):742–58.

128. Chao MP, Majeti R, Weissman IL. Programmed cell removal: a new obstacle in the road to developing cancer. Nat Rev Cancer. 2012;12(1):58–67.

129. Hadfield M, Chia F, Rice M. Growth and metamorphosis of planktonic larvae of *Ptychodera flava* (Hemichordata: Enteropneusta). In: Hadfield

M, editor. Settlement and metamorphosis of marine invertebrate larvae. New York: Elsevier; 1978. p. 247–54.

130. Brown FD, Tiozzo S, Roux MM, Ishizuka K, Swalla BJ, De Tomaso AW. Early lineage specification of long-lived germline precursors in the colonial ascidian *Botryllus schlosseri*. Development. 2009;136(20):3485–94.

131. De Mulder K, Kuales G, Pfister D, Willems M, Egger B, Salvenmoser W, et al. Characterization of the stem cell system of the acoel *Isodiametra pulchra*. BMC Dev Biol. 2009;9:69.

132. Agata K, Nakajima E, Funayama N, Shibata N, Saito Y, Umesono Y. Two different evolutionary origins of stem cell systems and their molecular basis. Semin Cell Dev Biol. 2006;17(4):503–9.

133. Shibata N, Hayashi T, Fukumura R, Fujii J, Kudome-Takamatsu T, Nishimura O, et al. Comprehensive gene expression analyses in pluripotent stem cells of a planarian, *Dugesia japonica*. Int J Dev Biol. 2012;56(1–3):93–102.

134. Hemmrich G, Khalturin K, Boehm A-M, Puchert M, Anton-Erxleben F, Wittlieb J, et al. Molecular signatures of the three stem cell lineages in hydra and the emergence of stem cell function at the base of multicellularity. Mol Biol Evol. 2012;29(11):3267–80.

135. Leclere L, Jager M, Barreau C, Chang P, Le Guyader H, Manuel M, et al. Maternally localized germ plasm mRNAs and germ cell/stem cell formation in the cnidarian *Clytia*. Dev Biol. 2012;364(2):236–48.

136. Funayama N. The stem cell system in demosponges: Suggested involvement of two types of cells: Archeocytes (active stem cells) and choanocytes (food-entrapping flagellated cells). Dev Genes Evol. 2013;223(1–2):23–38.

137. Solana J. Closing the circle of germline and stem cells: the Primordial Stem Cell hypothesis. EvoDevo. 2013;4(1):2.

138. Collins JJ, Wang B, Lambrus BG, Tharp ME, Iyer H, Newmark PA. Adult somatic stem cells in the human parasite *Schistosoma mansoni*. Nature. 2013;494(7438):476–9.

139. Chia FS, Rice K. Settlement and metamorphosis of marine invertebrate larvae. In: Chia FS, editor. Symposium on settlement and metamorphosis of marine invertebrate larvae (1977: Toronto, Ont). Amsterdam: Elsevier; 1978.

140. Emlet RB. Larval form and metamorphosis of a "primitive" sea urchin, *Eucidaris thouarsi* (Echinodermata: Echinoidea: Cidaroida), with implications for developmental and phylogenetic studies. Biol Bull. 1988;174(1):4–19.

141. Davidson EH, Peterson KJ, Cameron RA. Origin of bilaterian body plans: evolution of developmental regulatory mechanisms. Science. 1995;270(5240):1319–25.

142. Bird AM, von Dassow G, Maslakova SA. How the pilidium larva grows. EvoDevo. 2014;5(1):13.

143. Guha A, Lin L, Kornberg TB. Organ renewal and cell divisions by differentiated cells in *Drosophila*. Proc Natl Acad Sci. 2008;105(31):10832–6.

144. Nakayama-Ishimura A, Chambon J, Horie T, Satoh N, Sasakura Y. Delineating metamorphic pathways in the ascidian *Ciona intestinalis*. Dev Biol. 2009;326(2):357–67.

145. Tanaka K, Truman JW. Development of the adult leg epidermis in *Manduca sexta*: contribution of different larval cell populations. Dev Genes Evol. 2005;215(2):78–89.

146. Patry WL, Bubel M, Hansen C, Knowles T. Diffusion tubes: a method for the mass culture of ctenophores and other pelagic marine invertebrates. PeerJ. 2020;7(8): e8938.

147. Zhu A, Ibrahim JG, Love MI. Heavy-tailed prior distributions for sequence count data: removing the noise and preserving large differences. Bioinformatics. 2019;35(12):2084–92.

148. Anders S, Huber W. Differential expression analysis for sequence count data. Genome Biol. 2010;11:12.

149. Lowe CJ, Tagawa K, Humphreys T, Kirschner M, Gerhart J. Hemichordate embryos procurement, culture, and basic methods. In: Lowe CJ, editor. Methods in cell biology development of sea urchins, ascidians, and other invertebrate deuterostomes experimental approaches, vol. 74. Cambridge: Academic Press; 2004. p. 171–94.

150. Kuehn E, Clausen DS, Null RW, Metzger BM, Willis AD, Özpolat BD. Segment number threshold determines juvenile onset of germline cluster expansion in *Platynereis dumerilii*. J Exp Zoolog B Mol Dev Evol. 2021;58:403.

151. Edgar RC. MUSCLE: multiple sequence alignment with high accuracy and high throughput. Nucleic Acids Res. 2004;32(5):1792–7.

152. Huelsenbeck JP, Ronquist F. MRBAYES: Bayesian inference of phylogenetic trees. Bioinformatics. 2001;17(8):754–5.

153. Bruce H, Jerz G, Kelly S, McCarthy J, Pomerantz A, Senevirathne G, et al. Hybridization chain reaction (HCR). In Situ Protoc. 2021. https://doi.org/10.17504/protocols.io.bunznvf6.

154. Choi HMT, Schwarzkopf M, Fornace ME, Acharya A, Artavanis G, Stegmaier J, et al. Third-generation *in situ* hybridization chain reaction: multiplexed, quantitative, sensitive, versatile, robust. Development. 2018;145(12): dev165753.

Publisher's Note